FLOW FIELD IN THE CLOSE VICINITY OF A PROPELLER IN STATIC CONDITION AND ITS APPLICATION FOR MEASUREMENT OF STATIC THRUST

A thesis submitted

In Partial Fulfilment of the requirements

for the degree of

MASTER OF TECHNOLOGY

By

Squadron Leader K. P. Sharma

to the

Th
AE/1969/M
Sh23f

DEPARTMENT OF AERONAUTICAL ENGINEERING

INDIAN INSTITUTE OF TECHNOLOGY KANPUR

MAY, 1969

Tech

190

FLOW FIELD IN THE CLOSE VICINITY OF A PROPELLER IN STATIC CONDITION AND ITS APPLICATION FOR MEASUREMENT OF STATIC THRUST

A thesis submitted

In Partial Fulfilment of the requirements

for the degree of

MASTER OF TECHNOLOGY

JUNE '76

ACC NO - 190

By

Squadron Leader K. P. Sharma

AE-1969-M-SHA-FLOW

to the

DEPARTMENT OF AERONAUTICAL ENGINEERING

INDIAN INSTITUTE OF TECHNOLOGY KANPUR

MAY, 1969

CERTIFICATE

Certified that this work "Flow Field in the Close Vicinity of a Propeller in Static Condition and its Application for Measurement of Static Thrust" has been carried out under my supervision and that this has not been submitted elsewhere for a degree.

S.M. Ramachandra

S.M. RAMACHANDRA
Professor, Department of
Aeronautical Engineering
Indian Institute of Technology
Kanpur

ACKNOWLEDGEMENT

The author is greatly indebted to Dr. S.M. Ramachandra for the invaluable guidance and the keen interest shown throughout the course of this work.

The author is very grateful to Squadron Leader I.S. Gupta, his colleague at Indian Institute of Technology, Kanpur for devoting his precious time while carrying out the experimental work. The author's sincere thanks are also due to Mr. C.V.R. Murti and Mr. R.K. Bera for writing out the computer programme and making their valuable criticisms at various stages of the work. The author expresses his gratitude to Wing Commandar N.W. Tilak, Chief Pilot Instructor at I.I.T. for running the propeller as and when required. Last but not least the author acknowledges the kind help given by Messers S. Haque, R. Krishnamurthy and their staff in Flight Research Laboratory of I.I.T. without which the experimental work would have been incomplete.

CONTENTS

		Page
	SUMMARY	i
	LIST OF NOTATIONS	ii - iv
	LIST OF FIGURES	v
1.	INTRODUCTION	1
2.	CHAPTER 2	
	Analytical Formulation of Problem	5
3.	CHAPTER 3	
	3.1 Method of Solution	8
	3.2 Calculation of Z Component w of Induced Velocity	12
	3.3 Calculation of X Component U of Induced Velocity	14
	3.4 Calculation of Y Component v of Induced Velocity	15
	3.5 Calculation of Thrust	16
4.	CHAPTER 4	
	4.4 Experimental Setup and Measurements	20
	4.2.1 Measurement of Static Thrust by Wake Survey	23
	4.2.2 Measurement of Chord and Blade Angle	24
	4.3 Measurement of Static Thrust by Application of Directo Mechanical Methods	25
	4.4 Wake Survey by Pitch and Yawmeter	26
5.	CHAPTER 5: Discussion of Results	27
	5.1 Flow Field Behind the Propeller in its Close Vicinity	27
	5.2 Estimation of Propeller Static Thrust	28
	5.3 Flow Direction Behind the Propeller	30
6.	CHAPTER 6	
	6.1 Conclusion	32
	6.2 Suggestions	32
7.	APPENDICES I - VII	33 - 43
	REFERENCES	44 - 45

SUMMARY

The flow field in the close vicinity of the propeller in static condition $\frac{V}{nD} = 0$ has been analysed both experimentally and theoretically. The static thrust of the propeller has been measured by the wake survey method as well as by direct mechanical methods.

A complete solution has been obtained for all the three components of the induced velocity close to the propeller $Z \simeq 0$ for an arbitrary harmonic variation of vorticity as function of propeller radius. The Fourier constants have been determined from the circulation variation obtained from experimental data for the propeller. These constants have been used to estimate the coefficient of thrust C_T. There is a close agreement between the predicted values and the one obtained experimentally.

LIST OF NOTATIONS

P	Arbitrary point in space
R	Total radius of the propeller in inches
r	Vortex element radius measured parallel to tip path plane from wake axis
ϖ	Nondimensionalised radial distance $(\frac{r}{R})$ with respect to R
$\bar{q}$	Vector induced velocity at an arbitrary point P
$\bar{a}$	Vector distance from point P in space to vortex element
$d\bar{s}$	Vortex element
$\bar{s}$	Vector distance from origin to surface of the wake
X,Y,Z	Cartesian coordinate system centred in propeller, X positive upward, Y positive on the starboard side of aircraft and Z positive forward.
x, y, z	Cartesian coordinates of point P
ξ, η, ζ	Nondimensionalised coordinates of point P with respect to blade radius R $(\frac{x}{R}, \frac{y}{R}, \frac{z}{R})$
l	Running coordinate along the edge of the wake
$\bar{i}, \bar{j}, \bar{k}$	Unit direction vectors along X-,Y- and Z- axis respectively
u, v, w	Induced velocity components directed parallel to X-,Y- and Z- axis respectively
u', v', w'	Normalised incremental induced velocity components with respect to ωR directed parallel to X-,Y- and Z- axis respectively.
Γ	Blade circulation
Γ_0	Some constant circulation
Γ_*	A constant (ωR^2) having dimension of circulation
Γ'	Circulation normalised with respect to Γ_*
Γ_0'	Circulation normalised with respect to Γ_*

LIST OF NOTATIONS (Continued)

U_T	Tangential component of resultant velocity at blade element (ωr)
V	Forward speed of propeller
n	Revolution per minute of propeller
D	Diameter of propeller
ψ	Azimuth angle measured in direction of rotation from axis of X
$P_n(\mu)$	Legendre's polynomials
M	Mass of air
T	Thrust of propeller
C_T	Coefficient of thrust
L	Lift developed by propeller blade
ρ	Mass density of air slugs
ρ_w	Mass density of liquid used in the manometer
b	No. of propeller blades
Φ	Velocity potential
φ	Inflow angle
θ	Pitch angle
α	Effective incidence angle
c	Blade chord
U	Resultant air velocity
C_L	Coefficient of lift
a_0	Lift curve slope
C_d	Coefficient of drag
V_T	Rotor tip speed
C_p	Coefficient of pressure
h	Height of liquid column in the manometer tube
	Acceleration due to gravity

LIST OF NOTATIONS (Continued)

G	Constant factor for a given propeller
χ	$= \pi \tilde{\omega}$
$f(\chi)$	Fourier Sine series normalised with respect to the constant term describing the variation of vorticity along the radius.
$f'(\chi)$	The derivative of $f(\chi)$ with respect to χ
m	An integer
A_m	Normalised Fourier constant
a_m	$= m A_m$

LIST OF FIGURES

Fig. No.	Title
2.1.1	Assumed wake
2.1.2	Concentric circular vortex rings
2.1.3	Single vortex ring
2.1.4	Helical vortex rings
2.1.5	Trailing vortices shed due to incremental variation in circulation
3.5.1	Forces and velocities at blade element
4.1.1	Station designation in propeller wake
4.2.1	Kanpur II aircraft
4.2.2	Chord and blade angle variation of the propeller
4.2.3	Kanpur II aircraft with the pitot comb
4.2.4	Instrumentation in the cockpit of the aircraft
4.3.1	Spring balance complex attached to aircraft tailwheel
4.3.2	Strain gauge and strain gauge indicator
4.3.3	Strain gauge calibration curve
4.4.1	Pitch and Yawmeter installation
4.4.2	Pitch and Yawmeter calibration in wind tunnel
4.4.3	Calibration curve pitch and yawmeter
5.1.1	Variation of C_T with respect to ϖ^2
5.2.1	Pressure rise along propeller radius
5.2.2	Circulation variation along radius
5.2.3	Variation of propeller static thrust with respect to RPM
5.2.4	Variation of static thrust with respect to ϖ^2
5.3.1	Flow direction in the wake
5.3.2	Slipstream inclination

CHAPTER 1

Introduction

The characteristics of propellers in static condition become important to calculate the nosing over moments and in estimation of take off runs. It is, therefore, essential to obtain accurate static thrust and torque of a full scale propeller with zero forward velocity. In a wind tunnel it is quite difficult to achieve zero advance ratio condition due to the fact that the propeller itself creates a considerable air velocity through the tunnel and is also subjected to the constriction effects of the solid boundaries of the wind tunnel.

Diehl[1] (1932) has collected a great deal of static thrust data mostly extrapolated from wind tunnel tests for a large group of propellers. His calculations of static thrust are based on constants derived from Durand and Lasley's[2] (1920) tests on wooden propellers. Diehl[3] (1932) has used these results to estimate the take off distances of airplanes. Some useful static thrust data is also given by Louis[4] (1937). Unfortunately the material given in these references is not sufficient for a detailed estimation of propeller characteristics. Driggs[5] (1938) has developed a method by means of which test data for a propeller obtained in a wind tunnel can easily be converted to aerofoil coefficients representing the propeller based on the assumption that the differential thrust and differential torque coefficients $\left(\frac{dC_T}{d(\bar{\omega})^2}\right)$ and $\left(\frac{dC_Q}{d(\bar{\omega})^2}\right)$ respectively when plotted against $\bar{\omega}^2$ produce curves which are semiellipses. This simplifies the expression to the extent that the total thrust and the total torque coefficients are merely the product of $\frac{\pi}{4}$ and the derivatives $\left(\frac{dC_T}{d(\bar{\omega})^2}\right)$ and $\left(\frac{dC_Q}{d(\bar{\omega})^2}\right)$ at $\bar{\omega}^2 = 0.5$. The station representing the whole propeller is thus found

to be $\tilde{\omega}^2 = \left(\frac{r}{R}\right)^2 = 0.5$ or $\tilde{\omega} = \frac{r}{R} = 0.707$ and is for convenience, taken as the station at 0.7R. Conversely the thrust and torque gradients $\left(\frac{dC_T}{d(\tilde{\omega})^2}\right)$ and $\left(\frac{dC_Q}{d(\tilde{\omega})^2}\right)$ at 0.7R station may be easily obtained if the total thrust and torque coefficients C_T and C_Q are known from propeller tests. However, this theory limits itself to propellers without bodies inspite of the fact that this analysis has been used fairly successfully for wind tunnel tests of most of the propellers provided that the hub and cylindrical blade shanks are covered by a spinner. Montgomery and Hafner[6] (1937) have carried out a very satisfactory analysis of the static thrust of lifting airscrews both experimentally and theoretically. The experimental results obtained by them agree well with theoretical calculations. The theoretical aspect has been analysed on the basis of vortex theory with the assumptions that the mathematical model has infinite number of blades with small inflow angles neglecting rotational and radial components of induced velocity and slip stream contraction. The main feature of this work is that the solidity as an independent parameter has been eliminated. At the same time this analysis is valid only for an evaluation of constant pitch or constant chord rotors.

Some research agencies in the late fifties started focusing interest on the static thrust of propeller especially after the subject of propeller driven VTOL aircraft started to receive a considerable attention. Coward[7] (1957) gives a general method for establishing boundary conditions whereby a high efficiency under both static and forward flight conditions may be realized. Coward[8] (1959) also has given some data which yield a rapid, simple and sufficiently accurate estimation of static thrust of propellers of conventional design for most preliminary analysis.

The purpose of present analysis is to study the flow field in the close vicinity of a propeller using the measurements of the pressure and velocity distributions behind a Hartzell metallic propeller coupled to a Lycoming 250 HP engine mounted on a four place aircraft Kanpur II. The vortex theory is used to obtain the circulation distribution. Static thrust measurements have been made by tethering the aircraft.

The flow field behind the propeller as such is of very complex nature. There is a considerable difference between the flow in static condition and the flow that exists when the propeller is moving or when the propeller is placed in a wind tunnel airstream. In the static condition the propeller tips are working in a strong vortex that tends to reduce the effective aspect ratio of the propeller. Based on the vortex theory concept a great deal of work has been done on propellers and various correction factors have been determined. Mostly this analysis has been confined to the Betz[9] (1919) optimum condition for lightly loaded propellers neglecting the slipstream contraction and the periodicity of flow. This is equivalent to assuming that the number of blades is large. Prandtl[9] (1919) had developed a correction factor for a finite number of blades. Goldstein[10] (1929) has found out an expression for the circulation for lightly loaded propellers dealing with the conditions in the final wake. His basic assumption is that the velocity field of the vortex system at a large distance behind the airscrew is equivalent to the potential field of the rigid helicoidal surfaces. This solution when applied to the general problem is rigorously correct only for airscrews where the distribution of circulation along the blade is such that the flow in the wake is identical with the potential flow of such a set of equidistant coaxial helicoidal surfaces. It also assumes that

the path of the trailing vortices, making up helicoidal sheets coincides with the resultant velocity. Theodorsen[11] (1944) has shown that the vortex theory can be extended to heavily loaded propellers by applying a correction factor to the slipstream contraction.

In the present paper effort has been made to determine the velocity distribution in the close vicinity of the propeller by assuming the variation of circulation along the radius of the propeller in the form of a Fourier series. The Fourier coefficients have been computed from experimental data.

In Chapter 2 of the present thesis a mathematical formulation of the static thrust problem of a propeller is described. A mathematical model has been developed based on the usual assumptions made in the past with some modifications. In Chapter 3 this mathematical model is solved. Chapter 4 has been devoted to study the problem experimentally for correlating the results with the theory developed. An expression has been found relating circulation with the rise in pressure behind the propeller. The experimental results obtained have been discussed in Chapter 5 while the conclusions of the present work have been given in Chapter 6 together with suggestions for further investigations.

CHAPTER 2

Analytical Formulation of Problem

The flow field behind a propeller is of a highly complex nature. It is difficult to formulate a complete mathematical model and obtain its solution in its entirety taking into account this complicated flow field. Satisfactory results have been obtained for any design problem by resorting to various assumptions.

Since the propeller has no forward motion under static conditions and further since the axial velocity of the air is small compared to its rotational velocity the vortex filament shed from the propeller blade move in helical paths whose pitch angles are nearly zero. We may, therefore, assume that the wake of a static propeller is composed of an infinite number of concentric circular vortex rings of constant strength forming continuous semiinfinitely long vortex cylinder (Fig. 2.1.1). The case of helicopter rotors under hovering conditions away from the ground effect is closely similar to the case of a static propeller. This assumption is also equivalent to assuming an infinite number of blades forming the actuator disc. However, when the propeller is in forward motion this assumption may not be strictly valid especially for the usual operation range of of propellers. Close behind the propellers there exists a strong axial variation of the helix angle of the trailing vortex filaments. It is further assumed that the contraction in the slipstream is negligible. We shall assume that the circulation be constant in the azimuthal direction. Thus ensuring axial symmetry as is generally valid in the case of airplane propellers. However, this assumption is not valid in the case of helicopter rotors with forward velocity and propellers in flight moving in pitching or yawing attitude. In these cases it is necessary to take into account

both radial and azimuthal variation of circulation. Drees[12] (1949) has found an expression for the induced velocity of forward moving lifting rotors accounting for nonuniform azimuthal vorticity variation assuming however constant vorticity along the radius and infinite number of blades. This assumption is not significantly different from the actual case of static propellers because of the low wake velocities.

As mentioned above the slipstream of the static propeller may be regarded as an infinite series of coaxial circular vortex sheets (Fig. 2.1.2) parallel to the plane of the actuator disk. The vorticity of the sheet may be approximated by a series of closely spaced concentric vortex rings.

We consider first the case of a propeller having uniform circulation along the radius. This will produce a single helical vortex lying along a circular cylinder (Fig.2.1.3). In the far wake the induced velocity within the cylinder is uniform and there is no velocity induced at all outside the cylinder. In the case of varying circulation for an infinitesimal annulus of the actuator disc the wake is composed of two concentric circular cylinders having equal and apposite vorticity and separated by dr. The downwash between the two cylinders is uniform and proportional to the annulus loading. Everywhere else the downwash is zero. If the disk loading is made up of a continuous distribution of such annuli, the induced velocity directly downstream of each annulus is thus determined only by that annulus loading and is not affected by the loading of any other annulus. Hence the radial variation of the induced velocity is proportional to radial variation of the disk loading[13] (1956).

Because of the variation of circulation along the radius, trailing vortices spring from every point of trailing edge, thus forming

a vortex sheet of helicoid shape, the number of sheets being equal to the number of blades (Fig.2.1.4). The strength of each trailing vortex is determined from the circulation around the blade to satisfy Stoke's relation of continuity of vorticity. If $d\Gamma$ is the increase of circulation between points r and $r + dr$ of the blade, the strength of the helical vortex springing from this blade element will be $-d\Gamma$. Therefore the total circulation Γ at any radius may be considered as the sum of all the trailing vortices which leave the blade outside that radius (Fig. 2.1.5). As assumed by Heyson[14] (1959) the close spacing of these vortices converts the slipstream into a cylinder having a sheet of continuous vorticity. Hence the calculated induced velocities will be only the mean or time averaged velocities. The axial component of the vorticity which is important in case of helicopter rotor blades with forward motion is assumed to be negligible. This is equivalant to stating that the rotor tip speed is infinite so that the circulation is proportional to the local disk loading[15] (1960). Further the blade bound vortex is neglected since its average affect in the course of one revolution is zero.[14]

The essential part of the present analysis which is for a particular propeller condition, is that the wake vorticity variation along the radius is measured and incorporated in the analysis. As already stated the wake cylinder will be filled with radial vorticity of a strength proportional to radial derivative of the circulation. The equations which follow include all the three components of the induced velocity in the close viscinity of the propeller.

CHAPTER 3

3.1 Method of Solution

Let Γ be the circulation per unit length in the axial direction and it is expressed as

$$\Gamma = \Gamma_0 f(x) \tag{3.1.1}$$

where Γ_0 is the constant part of circulation and x is a function of . The elemental circulation per unit length along the coordinate ℓ will be given by

$$\frac{d\Gamma}{d\ell} = \frac{d\Gamma_0}{d\ell} f(x) \tag{3.1.2}$$

In normalised form with respect to Γ_* and the total radius R of propeller we have

$$\frac{\Gamma_*}{R} \times \frac{d\Gamma'}{d\ell'} = \frac{\Gamma_*}{R} \frac{d\Gamma_0'}{d\ell'} f(x) \tag{3.1.3}$$

Consider an element of a circular vortex ring of radius r at a vectorial distance $\bar{s}$. Let the width of the ring be $d\ell$. The circulation strength of the ring can be written as $\frac{d\Gamma}{d\ell} d\ell$. As the circulation along the radius is also changing the strength of elemental circulation will be given by $\frac{d}{dr}\left(\frac{d\Gamma}{d\ell}\right) d\ell$ where higher order terms of infinitesimals have been neglected.

In the first instance we consider only the constant part of the circulation i.e. the elemental ring with constant vorticity $\frac{d\Gamma_0}{d\ell} d\ell$

The velocity potential Φ due to such an element of vortex is given by[16]

$$\Phi = \frac{1}{4\pi}\iint \frac{d\Gamma_0}{dl}\, dl\, \frac{\cos\theta}{a^2}\, dA \tag{3.1.4}$$

Quantity $\frac{\cos\theta}{a^2} dA$ measures the elementary solid angle.

Therefore the velocity potential at point P can be written as

$$\Phi = \frac{1}{4\pi}\int_{l_1}^{l_2} \frac{d\Gamma_0}{dl}\beta\, dl$$ where β is the solid angle.

or

$$\Phi = \frac{d\Gamma_0}{dl}\frac{1}{4\pi}\left[\beta(l_2) - \beta(l_1)\right] \tag{3.1.5}$$

We consider the point P at the plane of rotor. Then for the entire cylinder $l_1 = 0$ and $l_2 = -\infty$

Therefore $\beta(l_2) = 0$ and $\beta(l_1) = 2\pi$

Substituting these values in (3.1.5) we have

$$\Phi = -\frac{1}{2}\frac{d\Gamma_0}{dl}\, l$$

so that

$$w_0 = \frac{d\Phi}{dl} = -\frac{1}{2}\frac{d\Gamma_0}{dl} \tag{3.1.6}$$

or in nondimensionalised form we have eq. (3.1.6) as

$$\frac{w_0}{\omega R} = -\frac{1}{2}\frac{d\Gamma_0'}{dl'} \tag{3.1.7}$$

Putting $\chi = \pi\tilde{\omega}$ we get

$$d\tilde{\omega} = d\left(\frac{r}{R}\right) = \frac{d\chi}{\pi} \tag{3.1.8}$$

For the limits when

$$r = 0 \qquad \tilde{\omega} = 0 \qquad \chi = 0$$

$$r = R \qquad \tilde{\omega} = 1 \qquad \chi = \pi \tag{3.1.9}$$

We shall assume the circulation to be represented by the Fourier series

$$\Gamma = \Gamma_0 f(\chi) = \Gamma_0 [A_0 + A_1 \sin\chi + A_2 \sin 2\chi + \cdots A_m \sin m\chi]$$

with the Fourier constants normalised with respect to the circulation Γ_0

$$\frac{d\Gamma}{d\ell} = \frac{d\Gamma_0}{d\ell}[A_0 + A_1 \sin\chi + A_2 \sin 2\chi + \cdots A_m \sin m\chi] \tag{3.1.10}$$

Now

$$\begin{aligned}\frac{d}{dr}\left(\frac{d\Gamma}{d\ell}\right) &= \frac{d}{d\chi}\left(\frac{d\Gamma}{d\ell}\right)\frac{d\chi}{dr} \\ &= \frac{d}{R\,d\left(\frac{r}{R}\right)}\left[\frac{\Gamma_*}{R}\,\frac{d\left(\frac{\Gamma}{\Gamma_*}\right)}{d\left(\frac{\ell}{R}\right)}\right] \\ &= \frac{\Gamma_*}{R^2}\,\frac{d}{d\tilde{\omega}}\left(\frac{d\Gamma'}{d\ell'}\right)\end{aligned} \tag{3.1.11}$$

Substituting for $d\tilde{\omega}$ from eq. (3.1.8) in equation (3.1.11) we have

$$\frac{d}{dr}\left(\frac{d\Gamma}{d\ell}\right) = \pi\frac{\Gamma_*}{R^2}\,\frac{d}{d\chi}\left(\frac{d\Gamma'}{d\ell'}\right) \tag{3.1.12}$$

Using eq.(3.1.2) we finally obtain

$$\frac{d}{dr}\left(\frac{d\Gamma}{dl}\right) = \pi \frac{\Gamma_*}{R^2} \frac{d\Gamma_0'}{dl'} f'(x)$$

Where $f'(x)$ denotes derivative of $f(x)$ with respect to x

$$= \frac{\Gamma_*}{R^2} \frac{d}{d\varpi}\left(\frac{d\Gamma'}{dl'}\right) = \pi \frac{\Gamma_*}{R^2} \frac{d\Gamma_0'}{dl'} \sum_{m=1}^{m=\infty} a_m \cos mx \qquad (3.1.13)$$

where $a_m = m A_m$

Now consider the effect of total circulation. The velocity induced by such a vortex ring at a point P is given by Biot-Savart's law as[17]

$$d\bar{q} = \frac{1}{4\pi} \frac{d}{dr}\left(\frac{d\Gamma}{dl}\right) \frac{d\bar{s} \times \bar{a}}{|\bar{a}|^3} dl \qquad (3.1.14)$$

From Fig.(2.1.1) we have

$$\bar{s} = \bar{i}(r\cos\psi) + j(r\sin\psi) + \bar{k}(-l)$$

Therefore

$$d\bar{s} = \left[\bar{i}(-r\sin\psi) + \bar{j}(r\cos\psi) + \bar{k}(0)\right] d\psi \qquad (3.1.15)$$

$$\bar{a} = \bar{i}(r\cos\psi - x) + \bar{j}(r\sin\psi - y) + \bar{k}(-l-z) \qquad (3.1.16)$$

Substituting the above in eq. (3.1.14) we have for the total velocity induced by the wake

$$\bar{q} = \frac{1}{4\pi}\int_0^{2\pi}\int_0^{R}\int_0^{\infty} \frac{\begin{vmatrix} \bar{i} & \bar{j} & \bar{k} \\ -r\sin\psi & r\cos\psi & 0 \\ r\cos\psi - x & r\sin\psi - y & -\ell - z \end{vmatrix} \, d\ell \cdot dr \cdot d\psi}{\left[(r\cos\psi - x)^2 + (r\sin\psi - y)^2 + (-\ell - z)^2\right]^{3/2}} \cdot \frac{d}{dr}\left(\frac{d\Gamma}{d\ell}\right) \qquad (3.1.17)$$

3.2 Calculation of Component w of Induced Velocity

From eq. (3.1.17) we obtain z component of induced velocity as

$$w = \frac{1}{4\pi}\int_0^{2\pi}\int_0^{R}\int_0^{\infty} \frac{d}{dr}\left(\frac{d\Gamma}{d\ell}\right)$$

$$\frac{\left[-r^2 + xr\cos\psi + yr\sin\psi\right] d\ell \cdot dr \cdot d\psi}{\left[r^2 + x^2 + y^2 + z^2 - 2r(x\cos\psi + y\sin\psi) + 2\ell z + \ell^2\right]^{3/2}} \qquad (3.2.1)$$

After integrating with respect to ℓ substituting limits and considering the flow field close to the propeller i.e. $z \approx 0$ eq. (3.2.1) yields (Appendix I)

$$w = \frac{1}{4\pi}\int_0^{2\pi}\int_0^{R} \frac{d}{dr}\left(\frac{d\Gamma}{d\ell}\right)$$

$$\frac{\left[-r^2 + xr\cos\psi + yr\sin\psi\right] dr \cdot d\psi}{\left[r^2 + x^2 + y^2 - 2xr\cos\psi - 2yr\sin\psi\right]} \qquad (3.2.2)$$

We nondimensionalise the eq.(3.2.2) with respect to R and substitute the values from eqs. (3.1.8 and 3.1.12)

$$w = \frac{\Gamma_*}{4\pi R}\int_0^{2\pi}\int_0^1 \frac{d}{d\varpi}\left(\frac{d\Gamma'}{d\ell'}\right) \frac{[-\varpi^2 + \xi\varpi\cos\psi + \eta\varpi\sin\psi]\, d\varpi \cdot d\psi}{\varpi^2 + \xi^2 + \eta^2 + 2\xi\varpi\cos\psi - 2\eta\varpi\sin\psi} \tag{3.2.3}$$

On integrating with respect to ψ and substituting the limits (Appendix II) eq. (3.2.3) yields

$$w = -\frac{\Gamma_*}{4R}\int_0^1 \frac{d}{d\varpi}\left(\frac{d\Gamma'}{d\ell'}\right) d\varpi \tag{3.2.4}$$

Substituting for $\frac{d}{d\varpi}\left(\frac{d\Gamma'}{d\ell'}\right)$ from eq. (3.1.13)

$$w = -\frac{\Gamma_*}{4R}\frac{d\Gamma_0'}{d\ell'}\sum_{m=1}^{m=\infty} a_m \int_0^{\pi} \cos m\chi \, d\chi \tag{3.2.5}$$

or

$$\frac{w}{\omega R} = -\frac{1}{4\pi}\frac{d\Gamma_0'}{d\ell'}\sum_{m=1}^{m=\infty} a_m \int_0^{\pi} \cos m\chi \, d\chi \tag{3.2.6}$$

or

$$w' = 0 \tag{3.2.7}$$

This indicates that the incremental normal component of induced velocity along the radius is zero.

3.3 Calculation of X Component U of Induced Velocity

From eq. (3.1.17) we obtain the X component of induced velocity as

$$U = -\frac{1}{4\pi}\int_0^{2\pi}\int_0^{R}\int_0^{\infty}\frac{d}{dr}\left(\frac{d\Gamma}{dl}\right)$$

$$\frac{[r\cos\psi(l+Z)\,dl\cdot dr\cdot d\psi}{[r^2+x^2+y^2+Z^2-2r(x\cos\psi+y\sin\psi)+2lZ+l^2]^{3/2}} \quad (3.3.1)$$

As in the previous case we substitute $Z \simeq 0$ and integrate with respect to l and substitute the limits the above equation yields (Appendix III)

$$U = -\frac{1}{4\pi}\int_0^{2\pi}\int_0^{R}\frac{d}{dr}\left(\frac{d\Gamma}{dl}\right)\frac{[r\cos\psi]\,dr\cdot d\psi}{[x^2+y^2+r^2-(2xr\cos\psi+2yr\sin\psi)]^{1/2}} \quad (3.3.2)$$

We nondimensionalise with respect to R and obtain

$$U = -\frac{\Gamma_*}{4\pi R}\int_0^{2\pi}\int_0^{1}\frac{d}{d\varpi}\left(\frac{d\Gamma'}{dl'}\right)\frac{[\varpi\cos\psi]\,d\varpi\cdot d\psi}{[\xi^2+\eta^2+\varpi^2-2\xi\varpi\cos\psi-2\eta\varpi\sin\psi]^{1/2}} \quad (3.3.3)$$

From appendix IV integration with respect to ψ yields

$$U = -\frac{\Gamma_*}{4R}\frac{\xi}{(\xi^2+\eta^2)}\int_0^{1}\frac{d}{d\varpi}\left(\frac{d\Gamma'}{dl'}\right)\varpi^2\,d\varpi \quad (3.3.4)$$

Substituting the value of $\frac{d}{d\varpi}\left(\frac{d\Gamma'}{dl'}\right)$ from (eq.3.1.14)

$$U = -\frac{\Gamma_*}{4\pi^2 R}\frac{d\Gamma_0'}{dl'}\frac{\xi}{(\xi^2+\eta^2)}$$

$$\sum_{m=1}^{m=\infty} a_m \int_0^{\pi} \chi^2 \cos m\chi \, d\chi \qquad (3.3.5)$$

From appendix V we have

$$U = \frac{\Gamma_*}{4\pi^2}\frac{d\Gamma_0'}{dl'}\frac{\xi}{\xi^2+\eta^2}\sum_{m=1}^{m=\infty} a_m \frac{2\pi}{m^2}$$

or

$$\frac{U}{\omega R} = U' = \frac{1}{2\pi}\frac{d\Gamma_0'}{dl'}\frac{\xi}{\xi^2+\eta^2}\sum_{m=1}^{m=\infty} a_m \frac{1}{m^2} \qquad (3.3.6)$$

(3.4.1)

3.4 Calculation of Y Component v of Induced Velocity

From eq. (3.1.17) we obtain the Y component of induced velocity as

$$v = -\frac{1}{4\pi}\int_0^{2\pi}\int_0^{R}\int_0^{\infty}\frac{d}{dr}\left(\frac{d\Gamma}{dl}\right)$$

$$\frac{[r\sin(l+z)]\,dr\cdot dl\cdot d\psi}{[r^2+x^2+y^2+z^2-2r(x\cos\psi+y\sin\psi)+2lz+l^2]^{3/2}} \qquad (3.4.1)$$

It may be seen that eq.(3.4.1) differs from eq.(3.3.1) in respect of only trigonometric term $\sin\psi$ and $\cos\psi$ in the numerator.

Hence solution of eq.(3.4.1) can be written as

$$v = -\frac{\Gamma_*}{4R}\frac{\eta}{\xi^2+\eta^2}\int_0^1 \frac{d\Gamma'}{d\varpi}\varpi^2 d\varpi \qquad (3.4.2)$$

or

$$\frac{v}{\omega R} = v' = \frac{1}{2\pi}\frac{d\Gamma_0'}{d\ell'}\frac{\eta}{\xi^2+\eta^2}\sum_{m=1}^{m=\infty} a_m \frac{1}{m^2} \qquad (3.4.3$$

3.5 <u>Calculation of Thrust</u>

The tangential component of the resultant velocity at the blade element is ωR (Fig. 3.5.1)

$$dT = \rho U_T \Gamma dr \qquad (3.5.1)$$

$$T = \rho b \int_0^R \int_0^\pi \omega r \Gamma_0 f(x)\, dx \cdot dr$$

From appendix VI we have

$$T = \rho b \frac{R^2}{2}\left[A_0\pi + 2\sum_{m=1}^{m=\infty}\frac{A_m}{m}\right]\omega\Gamma_0 \qquad (3.5.2)$$

or nondimensionalising eq.(3.5.2) by dividing both sides by

We have

$$C_T = \frac{b}{2}\frac{\Gamma_0'}{\pi}\left[A_0\pi + 2\sum_{m=1}^{m=\infty}\frac{A_m}{m}\right]$$

$$= \frac{b\Gamma_0' s}{2\pi} \quad \text{where } s = \left[A_0\pi + 2\sum_{m=1}^{m=\infty}\frac{A_m}{m}\right] \qquad (3.5.3)$$

The number of circular vortex elements formed per unit time at the rotor disk is $\frac{b\omega}{2\pi}$. The distance between the successive vortices is

$$d = \frac{2\pi r}{b} \sin \varphi \tag{3.5.4}$$

Since angle φ is quite small as already defined we have (Fig.3.5.1)

$$d = \frac{2\pi r}{b} \frac{w_0}{\omega r} = \frac{2\pi w_0}{b\omega} \tag{3.5.5}$$

$$\frac{d\Gamma}{dl} = \frac{d\Gamma_0}{dl} f(x) = \Gamma_0 f(x) \frac{b\omega}{2\pi w_0} \tag{3.5.6}$$

In nondimensional form we have

$$\frac{d\Gamma'}{dl'} = \frac{d\Gamma_0'}{dl'} f(x) = \Gamma_0' f(x) \frac{b\omega R}{2\pi w_0} \tag{3.5.7}$$

From eqs. (3.5.3) and (3.5.7) we have

$$\frac{d\Gamma_0'}{dl'} = C_T \frac{\omega R}{w_0} \frac{1}{s} \tag{3.5.8}$$

Substituting the value of $\frac{d\Gamma_0'}{dl'}$ from eq.(3.1.7) we have

$$\left(\frac{w_0}{\omega R}\right)^2 = \frac{C_T}{2} \frac{1}{s} \tag{3.5.9}$$

In rotor parameter the thrust is given by

$$T = \frac{\rho}{2} b \int_0^R C_L c\, \omega^2 r^2\, dr \tag{3.5.10}$$

Assuming $C_L = a_0 \alpha$ we can write eq.(3.5.9) in the form

$$T = \frac{\rho}{2} a_0 b \omega^2 \int \alpha c r^2 dr$$

Since

$$\alpha = (\theta - \varphi) \qquad \text{Fig. (3.5.1)}$$

$$T = \frac{\rho}{2} a_0 b \omega^2 \int_0^R (\theta - \varphi) c r^2 dr$$

In nondimensionalised form we have

$$C_T = \frac{a_0 b}{2\pi} \int_0^1 (\theta - \varphi) c' \tilde{\omega}^2 d\tilde{\omega} \qquad (3.5.11)$$

$$= \frac{a_0 b}{2\pi} \int_0^1 \left(\theta - \frac{w_0}{\omega R} \frac{1}{\tilde{\omega}}\right) c' \tilde{\omega}^2 d\tilde{\omega} \qquad (3.5.12)$$

From eqs.(3.5.9) and (3.5.12) we have

$$\left(\frac{w_0}{\omega R}\right)^2 = \frac{1}{2} C_T s = \frac{a_0 b s}{4\pi} \int_0^1 \left(\theta - \frac{w_0}{\omega R} \frac{1}{\tilde{\omega}}\right) c' \tilde{\omega}^2 d\tilde{\omega}$$

or

$$\left(\frac{w_0}{\omega R}\right)^2 = \frac{a_0 b s}{4\pi} \int_0^1 \theta c' \tilde{\omega}^2 d\tilde{\omega} - \frac{a_0 b s}{4\pi} \int_0^1 \frac{w_0}{\omega R} c' \tilde{\omega} d\tilde{\omega}$$

or

$$\lambda^2 + \frac{\lambda a_0 b s}{4\pi} \int_0^1 c' \tilde{\omega} d\tilde{\omega} - \frac{a_0 b s}{4\pi} \int_0^1 \theta c' \tilde{\omega}^2 d\tilde{\omega} \qquad (3.5.13)$$

Where $\lambda = \dfrac{w_0}{\omega R}$ (3.5.14)

$$\lambda^2 + A\lambda - B = 0$$

Solving the quadratic we have

$$\lambda = \frac{-A \pm \sqrt{A^2 + 4B}}{2} \tag{3.5.15}$$

The quantity on the right hand side of the above equation has to be positive

λ can be determined by evaluating A and B where

$$A = \frac{a_0 b s}{4\pi} \int_0^1 c' \varpi \, d\varpi \tag{3.5.16}$$

$$B = \frac{a_0 b s}{4\pi} \int_0^1 \theta c' \varpi^2 \, d\varpi \tag{3.5.17}$$

CHAPTER 4

4.1 Experimental Setup and Measurements

A propeller produces a pressure rise across the propeller disk. This may be related to the circulation distribution over the disk. We shall now obtain an expression for the pressure rise in terms of the circulation.[21] Strip theory can be used to obtain an expression for the induced velocity variation over a nonuniformly loaded propeller of arbitrary planform and twist. Consider an annulus of radius r and width dr (Fig. 3.5.1) of the propeller disk. We shall assume the inflow angle φ to be small so that

$$\sin\varphi = \tan\varphi = \varphi$$

Mass of air flowing through the annulus

$$M = 2\pi r\,(V_1 + w_0)\,dr \qquad (4.1.1)$$

Elemental thrust dT = elemental lift dL (4.1.2)

The total elemental lift for b number of propeller blades

$$= b \cdot dL = 2\pi r \rho (V_1 + w_0)\, 2 w_0\, dr$$

or

$$b\frac{dL}{d\bar{\varpi}} = 2\pi R^2 \rho (V_1 + w_0)\, 2 w_0 \bar{\varpi} \qquad (4.1.3)$$

In Fig. (4.1.1) station (1) is on the far upstream of the propeller. Stations (2) and (3) are the positions shown close to the propeller disk upstream and downstream respectively. Station (4) is on the far downstream in the propeller wake. Therefore we write

$$P_{T_1} = p_0 + \frac{1}{2}\rho V_1^2 \tag{4.1.4}$$

$$P_{T4} = p_0 + \frac{1}{2}\rho V_4^2 = p_0 + \frac{1}{2}\rho(V_1 + 2w_0)^2 \tag{4.1.5}$$

The rise in total pressure through the disk is

$$\Delta P_T = P_{T4} - P_{T1} = \frac{1}{2}\rho(4w_0 V_1 + 4w_0^2) = 2\rho w_0(V_1 + w_0) \tag{4.1.6}$$

Hence from eqs. (4.1.3) and (4.1.6) we have

$$b\frac{dL}{d\varpi} = \Delta P_T\, 2\pi R^2 \varpi \tag{4.1.7}$$

From vortex theory we have for the lift coefficient

$$C_L = \frac{\Gamma}{\frac{1}{2} c V_T \varpi} \tag{4.1.8}$$

So that

$$\frac{dL}{d\varpi} = \frac{1}{2}\rho V_T^2 \varpi^2 \tag{4.1.9}$$

From eqs.(4.1.7), (4.1.8), and (4.1.9) we have for the circulation at radius r

$$\Gamma = \frac{\Delta P_T\, 2\pi}{\rho\, \omega\, b} \tag{4.1.10}$$

Assuming circulation Γ and ΔP_T as function of ϖ we have from eq.(4.1.10)

$$\frac{\Delta P_T(\tilde{\omega})}{\omega} = \frac{\rho b}{2\pi}\Gamma(\tilde{\omega}) \tag{4.1.11}$$

We shall define a pressure coefficient C_P for this case by dividing both sides of (4.1.11) by $\frac{1}{2}\rho\omega R^2$ so that

$$C_P = \frac{\Delta P_T(\tilde{\omega})}{\frac{1}{2}\rho\omega^2 R^2} = \frac{\Gamma(\tilde{\omega})}{\omega R^2}\frac{b}{\pi} \tag{4.1.12}$$

or

$$C_P = \frac{b}{\pi}\frac{\Gamma(\tilde{\omega})}{\Gamma_*} = \frac{b}{\pi}\frac{\Gamma(\tilde{\omega})}{\Gamma_*} \tag{4.1.13}$$

where $\Gamma_* = \omega R^2$

since $\Delta P_T = \rho_w g h$ (4.1.14)

$$\frac{\rho_w g h}{\frac{1}{2}\rho\omega^2 R^2} = \frac{b}{\pi}\frac{\Gamma(\tilde{\omega})}{\Gamma_*} \tag{4.1.15}$$

or

$$\frac{\Gamma(\tilde{\omega})}{\Gamma_*} = G\frac{h}{\omega^2} \tag{4.1.16}$$

where $G = \dfrac{2\pi\rho_w g}{b\rho R^2}$ (4.1.17)

This establishes a direct relation between the circulation and the pressure rise across the propeller disk.

From eq. (4.1.7) we obtain for the elemental thrust dT over the element dr

$$dT = \Delta P_T \, 2\pi R^2 \bar{\omega} \, d\bar{\omega}$$

or

$$dT = 2\pi R^2 \bar{\omega} \rho_w g h \, d\bar{\omega} \qquad (4.1.18)$$

This can be integrated over the radius to get the total thrust.

4.2.1 Measurement of Static Thrust by Wake Survey

A 7' diameter metallic two bladed Hartzell propeller installed on a four place single engined aircraft Kanpur II has been used for this purpose. The propeller was connected to a Lycoming 250 HP engine (Fig. 4.2.1). Effort was made to obtain blade profile specifications and propeller characteristics from the manufacturers well in advance but the same could not be procured in time. The measured variation of the chord and blade angle has been plotted in (Fig. 4.2.2). Sixteen brass tubes of outer dia 0.069 in. and 6 in. long were mounted uniformly spaced 3 in. apart on a wooden strut spanning the complete radius of the propeller with four of the tubes projecting beyond the propeller disk. The rake was mounted on the top of the engine nacelle (Fig. 4.2.3) parallel to plane of the disk and at a distance of 3 ± 0.5 in. behind the plane of rotation on the axis of Z. Due to the safety requirements and installation difficulties a closer approach to the plane of rotation would eliminate the effects of tip vortex roll up in the outer wake for $\frac{V}{nD} = 0$ or the static propeller. After mounting the Pitot rake on the aircraft the position of the tubes along the radius was measured. Fifteen tubes (2-16) on the rake were

connected to a multimanometer with fifteen glass tubes. The first pitot was connected to micromanometer. Another micromanometer was connected to a tube fixed on the wing quite far from the propeller to observe the changes in the dynamic head of the free stream. The damping inherent in the combination of pressure tubes, manometer and the connecting tubing was sufficiently large to allow the assumption that the manometer readings represent the steady time averaged pressures.

The multimanometer and the micromanometers were kept in the cockpit (Fig. 4.2.4). After levelling it laterally the multimanometer was suspended with the help of a silk thread to ensure automatic verticality while the propeller was running. The two micromanometers were fixed in the cockpit and levelled before starting the engine. Distilled water was used in the manometers to indicate the pressure changes.

The tests were conducted by running the propeller at eight different rotational speeds (RPM 750, 1000, 1250, 1500, 1750, 2000, 2250 and 2400) with the blade pitch locked in the fine position.

4.2.2 Measurement of Chord and Blade Angle

An improvised method was been used to find the blade angle and the blade chord at the various blade stations. The aircraft was levelled up in lateral axis only. A big metallic plate (size 8'x4'x$\frac{1}{4}$") was kept under the propeller on the ground and properly levelled. With the help of a plumbob the propeller nose centre was fixed. This was finally used to place the propeller in a horizontal position. Projection of the farthest point on the plate from both the propeller blade tips adjudged by observation fixed the reference line on the plate placed on the ground. The propeller was then positioned in the longitudinal plane by setting the lower blade tip

at the minimum distance from the plate on the ground. At equal intervals projections from the plate were dropped on the leading and the trailing edges which in turn decided the farthest points on the aerofoil section of the blade. Finally the distance between these two points was measured with the help of vernier calipers giving the chord length at the section. The lines joining the two points on the ground plane corresponding to the blade chords were drawn and the angles with reference to the line joining the blade tip projections in the horizontal position were measured. The variation of blade chord and blade angle has been shown in Fig. (4.2.2).

4.3 Measurement of Static Thrust by Application of Direct Mechanical Methods

Two methods have been employed to measure the static thrust direct. In the first case three dynamometer type spring balances of 200 kg., 100 kg. and 100 kg. range were connected in parallel rigidly. The complete fitting with the help of ¼ in. SWR was connected to the tail wheel mounting (Fig.4.3.1) and a peg fixed in ground (not shown in the Fig.). The propeller was run at the same rotational speeds as mentioned in Sec. (4.2.1) and the thrust was recorded as indicated by the dynamometer spring balances. To ensure the reliability the spring balances were calibrated before hand.

In the second case the static thrust was measured with an SR4 strain gauge fixed on a calibrated (Fig. 4.3.2) mild steel specimen. The calibration curve of the strain gauge tension is shown in Fig. (4.3.3).

The thrust indicated by both the methods has been shown in Fig. (5.2.3).

4.4 Wake Survey by Pitch and Yawmeter

A 2 in. diameter five tube sphere type combined pitch and yawmeter was used to determine the direction of the airstream behind the propeller (Fig.4.4.1). The combined pitch and yawmeter was made out of a 2 in. diameter spherical brass ball. On the circular cross section four holes were drilled for pitch and yaw measurement and the fifth hole was in the centre to observe the total head. This pitch and yawmeter was mounted on a strut having streamlined shape fixed behind the propeller. A glass tube was fixed on the rake close to the yawmeter to measure the local static head.

The measurements have been taken by running the propeller at five different speeds (RPM 750, 1000, 1250, 1500, 1750). The pitch and yawmeter was shifted at four different positions on the rake along the radius. The pressure differneces were observed on the micromanometers installed in the airplane cabin. The combined pitch and yawmeter was calibrated in the 3'x2' low speed wind tunnel (Fig.4.4.2) of the department. The calibration curves of the yawmeter are shown in Fig.(4.4.3).

CHAPTER 5

Discussion of Results

5.1 Flow Field Behind the Propeller in its Close Vicinity

It will be observed from eq. (3.2.7) that the incremental normal component (w') of the induced velocity along the radius of the propeller disk is zero. This indicates that the normal component (w_0) of the induced velocity caused by the constant part of the circulation remains constant in the wake along the propeller so that $w_0 = -\frac{1}{2}\frac{d\Gamma_0}{dl}$ (eq. 3.1.6). Therefore it may be inferred that the normal component (w_0) of induced velocity in the propeller wake does not depend upon the variation in circulation along the blade radius. This condition will not occur in the case of propellers in pitch or yaw and helicopter rotors in forward flight. If in eq. (3.1.5) we choose a point P in the far wake the total solid angle subtended at P will be 4π so that the normal component of the velocity induced will be $\frac{d\Gamma_0}{dl} = 2\,w_0$. This is in quite close agreement with the momentum theory of the propeller. As seen from Fig. (5.1.1) the predicted static thrust is in close agreement with the measured static thrust for the wake assumed in Chapter 2.

Eqs. (3.3.6) and (3.4.3) show that the vertical and lateral components u and v respectively are symmetrical about the X and Y axis as has been assumed. Moreover both these components of the induced velocity do not play any part in the estimation of static thrust.

From an estimation of u', v' and w_0 it is possible to calculate the total velocity induced in the wake and hence the elemental pressure

distribution along the radius of the propeller in static condition can be determined.

5.2 Estimation of Propeller Static Thrust

The pressure rise behind the propeller in its close vicinity obtained from the wake survey has been shown in Fig. (5.2.1). The measured data are subject to the following corrections:

(a) Manometer Reservoir Correction

The multimanometer used has fifteen 0.145 in. diameter bore glass tubes connected to the two 0.5 in. diameter bore storage aluminium tubes. Let $h_1, h_2 \cdots h_{15}$ be the change in the level of the glass tube and H be the change in the liquid level of the storage tube. Then we have

$$\rho_w \frac{\pi d^2}{4} \sum_{n=1}^{n=15} h_n = 2 \rho_w \pi \frac{D^2}{4} H. \qquad (5.2.1)$$

or

$$H = \frac{d^2}{2D^2} \sum_{n=1}^{n=15} h_n \qquad (5.2.2)$$

Therefore the actual rise in pressure in one tube will be $h + H$

(b) Correction for Slipstream Contraction and Rotation

The rake should be installed on the aircraft behind the propeller in such a way that the probes should be as close as possible to the blade trailing edge. This will avoid the effects of slipstream contraction and rotation especially for $\frac{V}{nD} = 0$ as under such condition the propeller blade tips produce a very strong vortex field. In the present experimental analysis due to the installation difficulties the distance between the blade trailing edge and the probes could not be reduced below 3" ± 0.5". This is quite

large to cause considerable inaccuracy in the static thrust. However Lock[22] (1939) has accounted for the slipstream contraction. A method for the estimation of the correction factor for slipstream rotation has been given by Lock[23] (1932). Because of the nonavailability of these two reports it has not been possible to correct for rotation and contraction of the slipstream.

(c) Flow Inclination to the Pitot Comb

The total head readings of the tubes of the pitot comb have to be corrected for the local measured flow inclinations. This requires a calibration of the total head tube with yaw. For want of time this has not been done. The correction will be incorporated soon after the calibration has been made.

Fig. (5.2.2) shows the circulation variation over the blade (eq. 4.1.16) corrected for manometer reservoir level variations only. An arithmetical mean dimensionless circulation $\frac{\Gamma}{\Gamma_*}$ has also been shown in Fig. (5.2.2). The shaded portion in this Fig. (5.2.2) indicates the blade tip losses due to the rolling up of the blade tip vortices and the wake contraction. In normal cases when the propeller has some advance ratio $\frac{V}{nD} \neq 0$ the circulation curve should intersect the $\tilde{\omega}$ axis between $\tilde{\omega}$ = 0.95 and 1. The present experimental result substantiates the foregoing statement that the tip vortices are stronger in case of propellers with static condition as compared to propellers in forward flight.

For computational purpose the mean curve has been approximated at the root and the blade tip as shown. Due to the presence of the engine nacelle the first probe fixed at $\tilde{\omega}$ = 0.21 had too many nonperiodic fluctuations at all propeller speeds possibly due to the engine nacelle interference. Consequently the correct behaviour of air stream at this station could not

be obtained. Again probes situated beyond the propeller disk radius indicate a finite pressure rise possibly caused by the blade tip flow. However, this apparent residual circulation has also been neglected for computational purposes. The approximated mean curve has been used to compute the Fourier constants A_m using the least mean square fit. The computed Fourier constants (Appendix VII) have been used to estimate theoretically the coefficient of thrust (C_T) and normal component (W_e) of the induced velocity using eqs. (3.5.9), (3.5.15), (3.5.16) and (3.5.17) $\mathcal{A}$ and $\mathcal{B}$ have been obtained by numerical integration using Simpson's rule taking the measured values of (C') and (θ) from Fig. (4.2.5).

The static thrust estimated and those measured at eight different rotational speeds of the propeller using the three different methods of chapter (4.2.1) and (4.3) has been plotted against the rotational speeds of propeller (Fig. 5.2.3). Fig1(5.2.4) indicates the variation of thrust with respect to square of angular velocity $((\omega))$ of the propeller. Approximate correction for the 20 kg. dead load of the spring balance complex has been applied in respect of static thrust obtained by spring balance. Ground friction of 15 kg. has been accounted for in case of static thrust obtained by the spring balance method and the strain gauge method. Satisfactory linearity has been obtained with all the three methods.

Coefficient of thrust (C_T) calculated and theoretically predicted has been shown in Fig. (5.1.1). As may be observed both the values are in close agreement. It may, therefore, be stated that the present analysis gives a reliable estimate of the static thrust of propellers having varying chord and pitch distribution along the radius.

5.3 Flow Direction Behind the Propeller

It may be observed from Fig. (5.3.1) that the air stream has a

tendency to move inward indicating slipstream contraction. The contraction reduces as the RPM of the propeller increases and decreases as we go along the radius of the propeller from root to tip. This is quite consistant with the assumed wake in case of the propeller in static condition. This is quite distinct in Fig. (5.3.2) which indicates the inclination of slipstream both in yaw and pitch with respect to the plane of the propeller at various speeds.

It may be added that effort was made to measure both pitch and yaw exactly at the blade tip. The same has been found to be almost zero due to the slipstream contraction. However from Fig. (5.3.1) it is possible to estimate the rotational velocity in the slipstream of the propeller as shown in Fig. (5.3.2).

CHAPTER 6

6.1 Conclusion

A study of symmetry relations concerning the induced velocities in the plane of a nonuniformly loaded propeller in static condition indicates that:

1). The component (w_o) of the induced velocity in the axial direction of the propeller in the wake is constant along the radius and it does not depend upon the variation in circulation as a function of the propeller radius.

2). The induced velocity components in X and Y direction are symmetrical which is consistant with the assumed wake.

3). The static thrust of the propeller can quite accurately be computed in case the circulation variation as a function of the radius of the propeller be known. Conversely the pitch and chord of the propeller can be varied to obtain the desired static thrust.

6.2 Suggestions

It is possible to extend the provisions of the present study to the case of helicopter rotors in hovering condition as the flow field in the case of propellers in static condition and helicopter rotor blades in hovering have approximately similar characteristics. The experimental procedure with some modification can be utilised to study the characteristics of the wake and thrust developed by the rotors while operating in-ground effect and out-of-ground effect.

APPENDIX I

Solution of Integral 3.2.1

$$I = \int_0^\infty \frac{[-r^2 + xr\cos\psi + yr\sin\psi]\,dl}{[r^2 + x^2 + y^2 - 2r(x\cos\psi + y\sin\psi) + l^2]^{3/2}} \tag{1}$$

We make the following substitutions

$$\begin{aligned} A &\equiv -r^2 + xr\cos\psi + yr\sin\psi \\ a &\equiv r^2 + x^2 + y^2 - 2r(x\cos\psi + y\sin\psi) \\ b &\equiv 0 \\ c &\equiv 1 \\ q &\equiv 4ac - b^2 \end{aligned} \tag{2}$$

Hence eq.(1) reduces to the form

$$I = \int_0^\infty \frac{A}{(a + bl + cl^2)^{3/2}}\,dl \tag{3}$$

From item 167 reference (17)

$$I = A\left[\frac{2(cl + b)}{q\sqrt{a + bl + l^2}}\right]_0^\infty \tag{4}$$

Substituting the limits, eq. 4 yields

$$I = \frac{A}{(2\sqrt{ac} + b)\sqrt{a}} \tag{5}$$

APPENDIX I (Continued)

From eq. (2) we have

$$I = \frac{A}{a}$$

$$= \frac{(-r^2 + xr\cos\psi + yr\sin\psi)}{r^2 + x^2 + y^2 - 2r(x\cos\psi + y\sin\psi)} \qquad (6)$$

APPENDIX II

Evaluation of Integral 3.2.3

$$I=\int_0^{2\pi}\frac{[-\tilde{\omega}^2+\xi\tilde{\omega}\cos\psi+\eta\tilde{\omega}\sin\psi]\,d\psi}{\tilde{\omega}^2+\xi^2+\eta^2-2\xi\tilde{\omega}\cos\psi-2\eta\tilde{\omega}\sin\psi} \tag{1}$$

We make the following substitutions

$$\begin{aligned} A &\equiv -\tilde{\omega}^2 \\ B &\equiv \xi\tilde{\omega} \\ C &\equiv \eta\tilde{\omega} \\ a &\equiv \tilde{\omega}^2+\xi^2+\eta^2 \\ b &\equiv -2\xi\tilde{\omega} \\ c &\equiv -2\eta\tilde{\omega} \end{aligned} \tag{2}$$

Hence eq.(1) reduces to the form

$$I=\int_0^{2\pi}\frac{A+B\cos\psi+C\sin\psi}{a+b\cos\psi+c\sin\psi}\,d\psi \tag{3}$$

From item 2.558-2 reference 18 we obtain

$$I=\left[\frac{Bc-Cb}{b^2+c^2}\log(a+b\cos\psi+c\sin\psi)+\frac{Bb+Cc}{b^2+c^2}\right]_0^{2\pi}$$

$$+\left(A-\frac{Bb+Cc}{b^2+c^2}a\right)\int_0^{2\pi}\frac{d\psi}{a+b\cos\psi+c\sin\psi} \tag{4}$$

$$\int_0^{2\pi} \frac{d\psi}{a + b\cos\psi + c\sin\psi}$$

$$= \frac{1}{\sqrt{b^2+c^2-a^2}} \log \frac{(a-b)\,tg\frac{\psi}{2} + c - \sqrt{b^2+c^2-a^2}}{(a-b)\,tg\frac{\psi}{2} + c + \sqrt{b^2+c^2-a^2}} \quad \text{when } a^2 < b^2+c^2$$

$$= \frac{2}{\sqrt{a^2-b^2-c^2}} \, arc\,tg \frac{(a-b)\,tg\frac{\psi}{2} + c}{\sqrt{a^2-b^2-c^2}} \quad \text{when } a^2 > b^2+c^2$$

$$= \frac{1}{c} \log\left(a + c\,tg\frac{\psi}{2}\right) \quad \text{when } a = b. \qquad (5)$$

$$= \frac{-2}{c + (a-b)\,tg\frac{\psi}{2}} \quad \text{when } a^2 = b^2+c^2$$

In all the cases stated above integral (5) will be zero after substituting limits from 0 to 2π Therefore eq.(4) reduces to the form

$$I = \left[\frac{Bc - Cb}{b^2+c^2} \log(a + b\cos\psi + c\sin\psi) + \frac{Bb + Cc}{b^2+c^2}\psi\right]_0^{2\pi} \qquad (6)$$

On substituting the limits we obtain

$$I = \frac{Bb + Cc}{b^2 + c^2} 2\pi \qquad (7)$$

We substitute values from eq.(3)

$$I = \frac{-2(\xi^2\tilde{\omega}^2 + \eta^2\tilde{\omega}^2)}{4(\xi^2\tilde{\omega}^2 + \eta^2\tilde{\omega}^2)} 2\pi$$

$$I = -\pi \qquad (8)$$

APPENDIX III

Evaluation of Integral 3.3.1

$$I = \int_0^\infty \frac{(r\cos\psi)\, l \cdot dl}{\left[r^2 + x^2 + y^2 - 2r(x\cos\psi + y\sin\psi + l^2\right]^{3/2}} \quad (1)$$

We make the following substitutions

$$\begin{aligned} A &\equiv r\cos\psi \\ a &\equiv r^2 + x^2 + y^2 - 2r(x\cos\psi + y\sin\psi) \\ b &\equiv 0 \\ c &\equiv 1 \\ q &\equiv 4ac - b^2 \end{aligned} \quad (2)$$

Hence equ(1) reduces to the form

$$I = \int_0^\infty \frac{Al \cdot dl}{[a + bl + cl^2]^{3/2}}$$

From item 175 reference 17 we have

$$I = \left[-\frac{2(bl + 2a)}{q\sqrt{a + bl + cl^2}} \right]_0^\infty A \quad (3)$$

$$I = -A\left[\frac{b}{q\sqrt{c}} - \frac{2a}{q\sqrt{a}}\right]2$$

Substituting the values from eq.(2) we have

$$I = \frac{A}{\sqrt{a}} = \frac{r\cos\psi}{\sqrt{r^2 + x^2 + y^2 - 2r(x\cos\psi + y\sin\psi)}} \quad (4)$$

APPENDIX IV

Evaluation of Integral 3.3.3

$$I = \int_0^{2\pi} \frac{(\cos\psi)\, d\psi}{\sqrt{\xi^2 + \eta^2 + \varpi^2 - 2\xi\varpi\cos\psi - 2\eta\varpi\sin\psi}} \tag{1}$$

We make the following transformations

$$\xi^2 + \eta^2 \equiv \beta^2$$

$$\xi\cos\psi + \eta\sin\psi \equiv \lambda$$

$$\frac{\varpi}{\beta} \equiv h \tag{2}$$

$$\frac{\lambda}{\beta} \equiv \mu$$

Therefore

$$I = \int_0^{2\pi} \frac{\cos\psi}{\beta\sqrt{1 + h^2 + \mu h}}\, d\psi \tag{3}$$

or from reference 19 we have

$$I = \frac{1}{\beta}\int_0^{2\pi} \cos\psi \left[\sum_{n=0}^{n=\infty} P_n(\mu) h^n \right] d\psi$$

where

$$P_0(\mu) = 1$$

$$P_1(\mu) = \mu$$

$$P_2(\mu) = \frac{1}{2}(3\mu^2 - 1) \tag{4}$$

$$P_3(\mu) = \frac{1}{2}(5\mu^3 - 3\mu)$$

APPENDIX IV (Continued)

$$P_5(\mu) = \frac{1}{8}(63\mu^5 - 70\mu^3 + 15\mu)$$

$$P_6(\mu) = \frac{1}{16}(231\mu^6 - 315\mu^4 + 105\mu^2 - 5)$$

We substitute (4) in eq.(3) and integrate term by term.

$$I = \int_0^{2\pi} \cos\psi \left\{ 1 + \mu h + \frac{3}{2}\mu^2 h^2 - h^2 + \frac{5}{2}\mu^3 h^3 - \frac{3}{2}\mu h^3 \right.$$

$$\left. + \frac{35}{8}\mu^4 h^4 - 30\mu^2 h^4 + 3h^4 - \cdots\cdots \right\} d\psi \tag{5}$$

$$I_1 = \int_0^{2\pi} \cos\psi \, d\psi = \Big[\sin\psi\Big]_0^{2\pi} = 0 \tag{6}$$

$$I_2 = \frac{h}{\beta}\int_0^{2\pi} \cos\psi(\xi\cos\psi + \eta\sin\psi)\, d\psi$$

$$= \frac{h}{\beta}\left[\eta\frac{1}{2}\sin^2\psi + \xi\left(\frac{\psi}{2} + \frac{1}{4}\sin 2\psi\right)\right]_0^{2\pi}$$

$$= \frac{h}{\beta}\xi\pi \tag{7}$$

$$I_3 = \frac{1}{2}h^2\int_0^{2\pi}\left\{\frac{\cos\psi}{\beta^2}(\xi\cos\psi + \eta\sin\psi)^2 - \cos\psi\right\} d\psi$$

$$= \frac{1}{2}h^2\int_0^{2\pi}\frac{1}{\beta^2}\left\{\xi^2\cos^3\psi + \eta^2\cos\psi\sin^2\psi + \right.$$

$$\left. 2\xi\eta\cos^2\psi\sin\psi - \cos\psi\right\} d\psi$$

$$= 0 \tag{8}$$

APPENDIX IV (Continued)

Like-wise terms of all higher order are zero. Therefore,

$$I = \frac{h}{\beta} \xi \pi = \frac{\tilde{\omega}}{\beta^2} \xi \pi \tag{9}$$

or

$$I = \frac{\tilde{\omega}}{\xi^2 + \eta^2} \xi \pi \tag{10}$$

APPENDIX V

Evaluation of Integral $I = \int_0^{\pi} x^2 \cos mx \, dx$

$$I = \frac{1}{m}\left[\int_0^{\pi} x^2 \, d(\sin mx)\right.$$

$$= \frac{1}{m}\left[x^2 \sin mx + \frac{2}{m}\left\{x \cos x + \frac{1}{m}\sin mx\right\}\right]_0^{\pi}$$

$$= -\frac{2\pi}{m^2}$$

APPENDIX VI

Evaluation of Integral $\int_0^{\pi}\int_0^{R} r f(x)\, dx\, dr$

$$I = \int_0^{\pi} f(x) \left[\frac{r^2}{2} \right]_0^R dx$$

$$= \int_0^{\pi} \frac{R^2}{2} \left[A_0 + \sum_{m=1}^{m=\infty} A_m \sin mx \right] dx$$

$$= \frac{R^2}{2} \left[A_0 \pi + 2 \sum_{m=1}^{m=\infty} \frac{A_m}{m} \right]$$

APPENDIX VII

Following are the Fourier constants as computed.

$\tilde{\omega}$	$\left(\frac{10^{-4}}{G}\right) A_m$
0.00	1.753956
0.214	-0.178640
0.286	0.122000
0.315	0.383681
0.357	0.200718
0.428	0.479401
0.5	-0.065506
0.57	-0.006008
0.643	-0.448635
0.71	-0.306022
0.786	-0.462631
0.86	-0.255835
0.93	-0.172175
1.00	-0.137359

REFERENCES

1. Walter, S. Diehl:

   Static thrust of airplane propellers, NACA TR No.447 (1932)

2. Durand, W.F. and Lesley E.P:

   Experimental research on air propellers II, NACA TR No. 30 (1920)

3. Walter, S. Diehl:

   The calculation of take-off run, NACA TR No.450 (1932)

4. Enos Louis, H:

   Some full scale static propeller characteristics,
   Jour. Aero. Sci., Vol.5, No.1, pp 25-28 (Nov.1937)

5. Driggs, Ivan. H:

   Simplified propeller calculations,
   Jour. Aero. Sci., Vol.5, No.9, pp 337-344 (July 1938)

6. Montgomery Knight and Ralph, A. Hafner:

   Static thrust analysis of the lifting airscrews, NACA TND 626 (1937)

7. Coward, Ken. S:

   Propeller selection for high static and forward flight efficiency
   for VTOL aircraft, Aeronautical Engineering Review, Vol.16, No.7,
   pp 41-43 (July 1957)

8. Coward, Ken. S:

   Propeller static thrust aero/space engineering, pp 64-68 (March 1959)

9. Albert Betz:

   Screw propeller with minimum loss of energy with appendix
   by Prnadtl L. Vier Abhandlungen in der Aerodynamik schrauben
   Propeller mit geringsten energieverlust (1919)

10. Sydney Goldstein:

    On the vortex theory of screw propellers,
    Proc. Roy. Soc. (London), Ser. A, Vol. 123, No.792,
    pp 440-465 (April 6, 1929)

11. Theodore Theodorsen:

    The slipstream contraction with numerical values for two blade
    and four blade propellers, NACA TR No. 777 (1944)

REFERENCES (Continued)

12. Drees, J. Meijer;

A theory of airflow through rotors and its applications to some helicopter problems, Jour. Helicopter Assoc. of Great Britain, Vol.3, No.2, July-Aug., pp 79-104 (Sept. 1949)

13. Heyson,Harry H. and S. Katzoff:

Normal component of Induced velocity in the vicinity of a lifting rotor with a nonuniform disk loading, NASA TND 3690 (1956)

14. Heyson, Harry. H:

Induced flow near a helicopter rotor, Aircraft Engineering, Vol. XXXI, No.360, pp 40-44 (Feb. 1959)

15. Heyson, Harry. H:

A note on the mean value of induced velocity for a helicopter rotor, NASA TND No.240 (1960)

16. Sir Horace Lamb:

Hydrodynamics, Sixth edition, Dover publication (1932)

17. A Robinson and J.A. Laurmann:

Wing Theory, Cambridge Aeronautics series.

18. Peirce, B.O. and Ronald, M. Foster:

A short table of integrals, Fourth edition, Oxford and IBM Publishing Co.

19. Gradshteyn, I.S. and Ryzhik, I.M:

Table of integral series and products, Academic Press, New York and London.

20. Louis, A. Pipes:

Applied mathematics for engineers and physicists, McGraw-Hill Book Co., New York.

21. Payne, P.R.:

Helicopter dynamics and aerodynamics, Sir Isaac Pitman & Sons, Ltd., London (1959)

22. Lock, C.N.H. and Bateman,H. and Nixon, H.L:

Measurement of thrust and torque grading on high pitch model screws, R & M 2477 (1939)

23. Lock, C.N.H. and Yeatman, D:

Theoretical cruves illustrating the periodic flow behind an airscrew. R & M 1483 (1932)

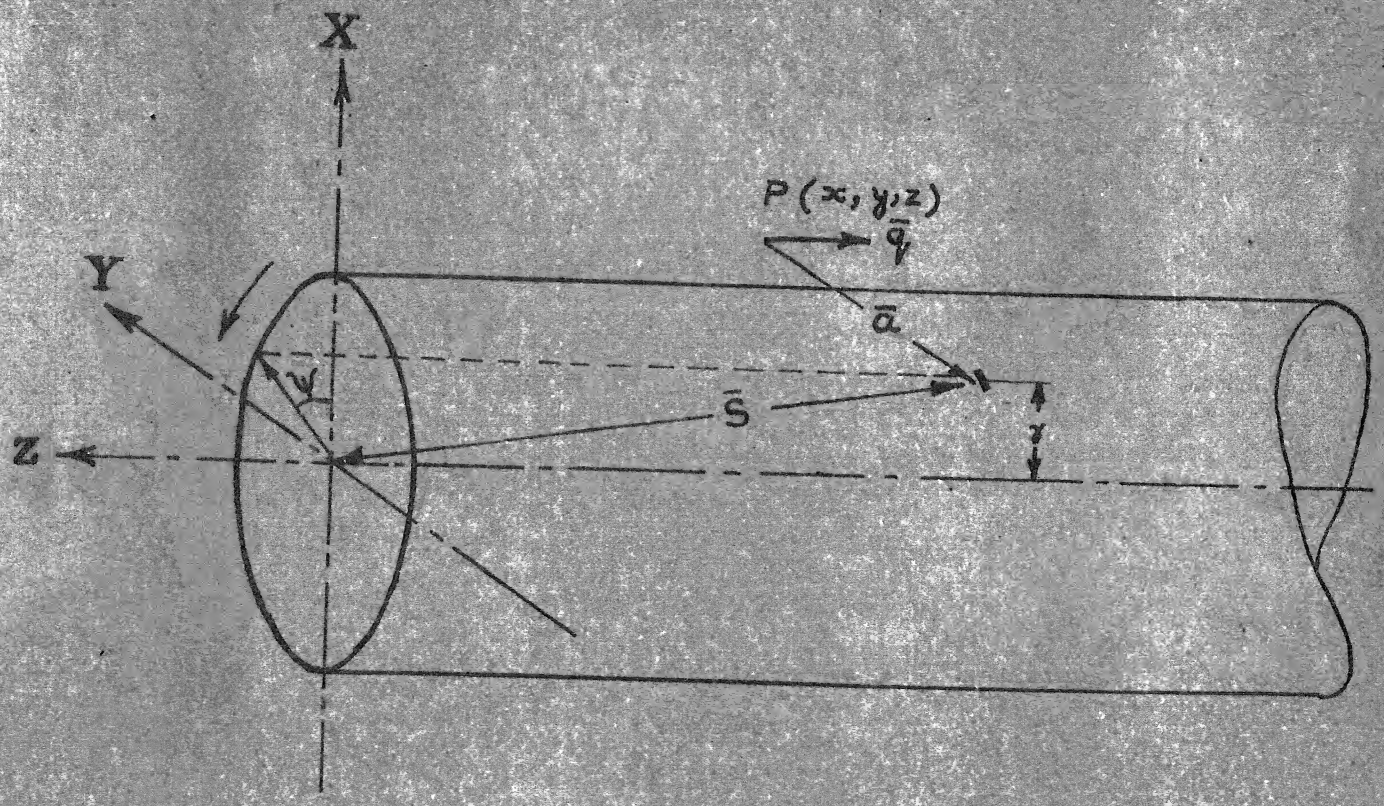

FIG. (2·1·1) ASSUMED WAKE

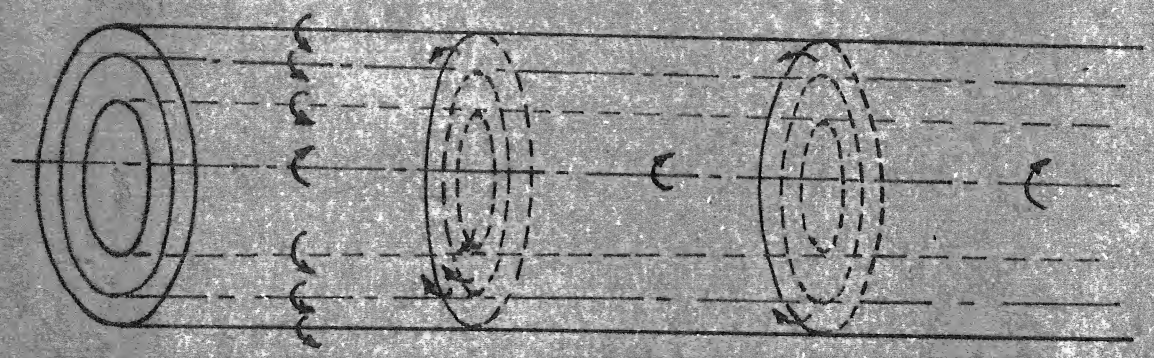

FIG. (2·1·2) CONCENTRIC CIRCULAR VORTEX RINGS

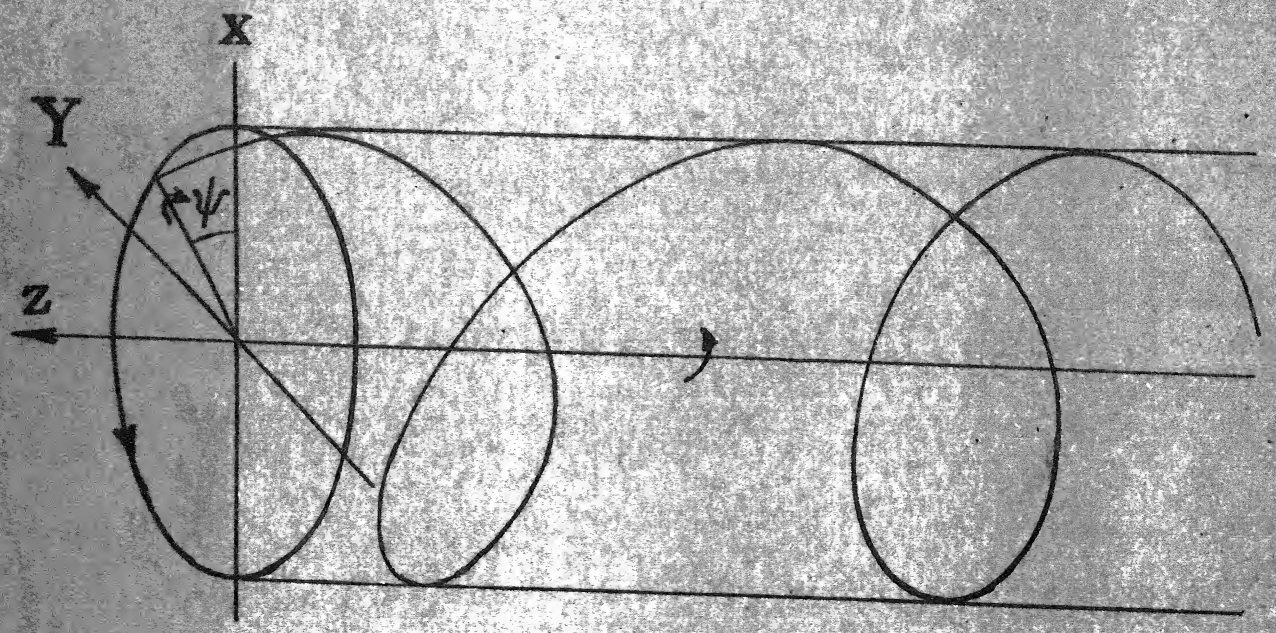

FIG. (2·1·3) SINGLE VORTEX RING

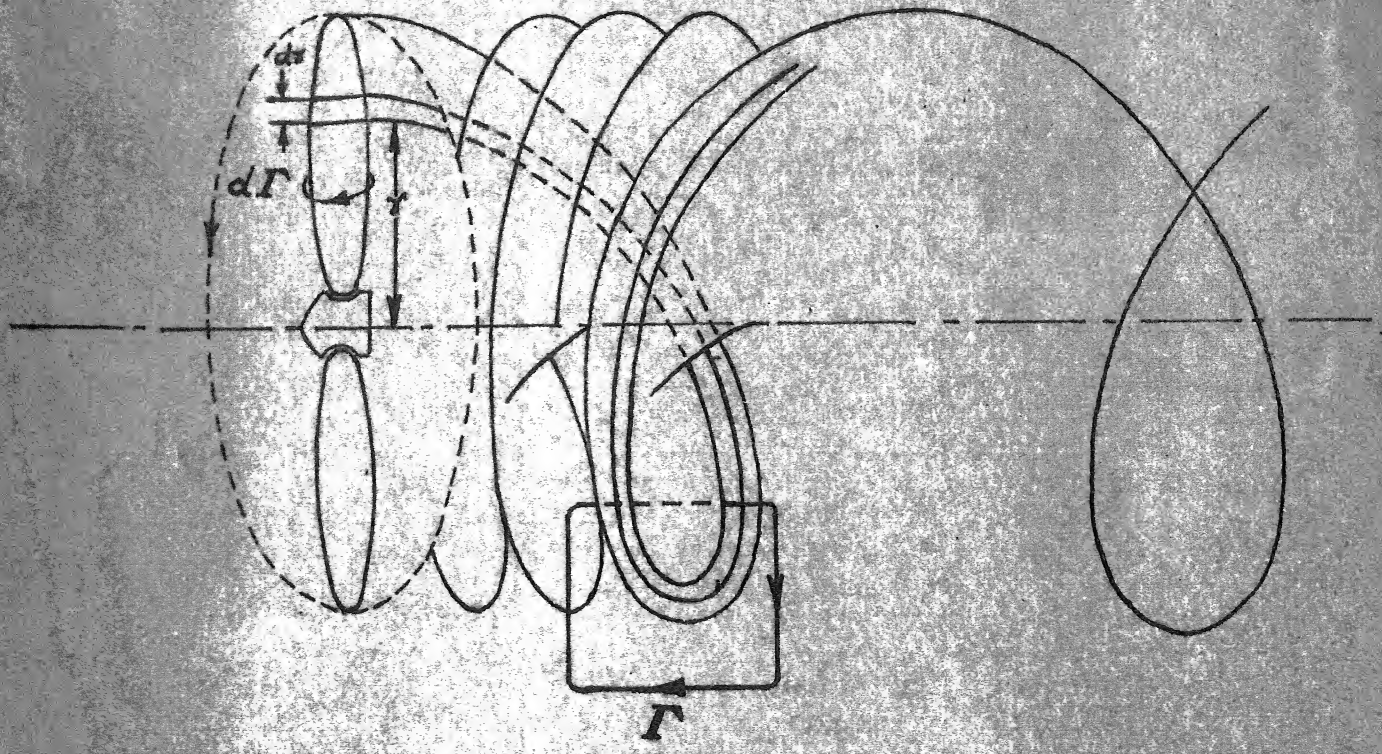

FIG. (2·1·4) HELICAL VORTEX RINGS

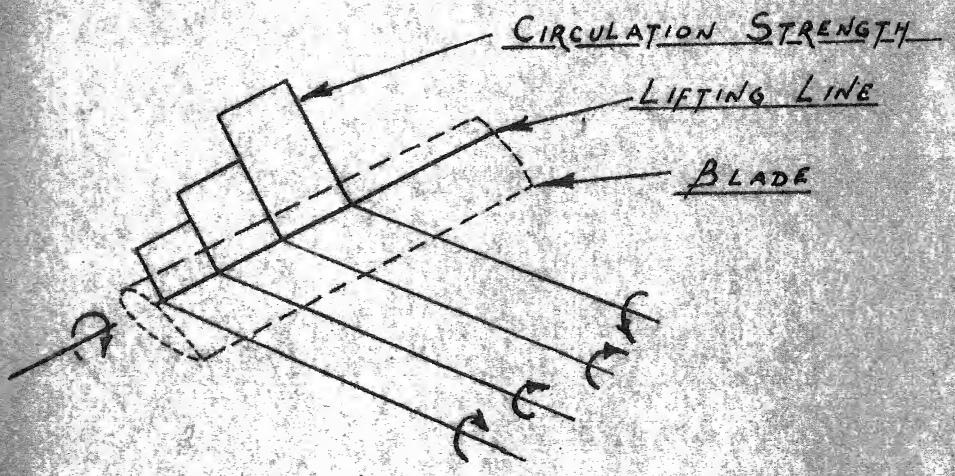

FIG. (2.1.5) TRAILING VORTICES SHED DUE TO INCREMENTAL VARIATION IN CIRCULATION

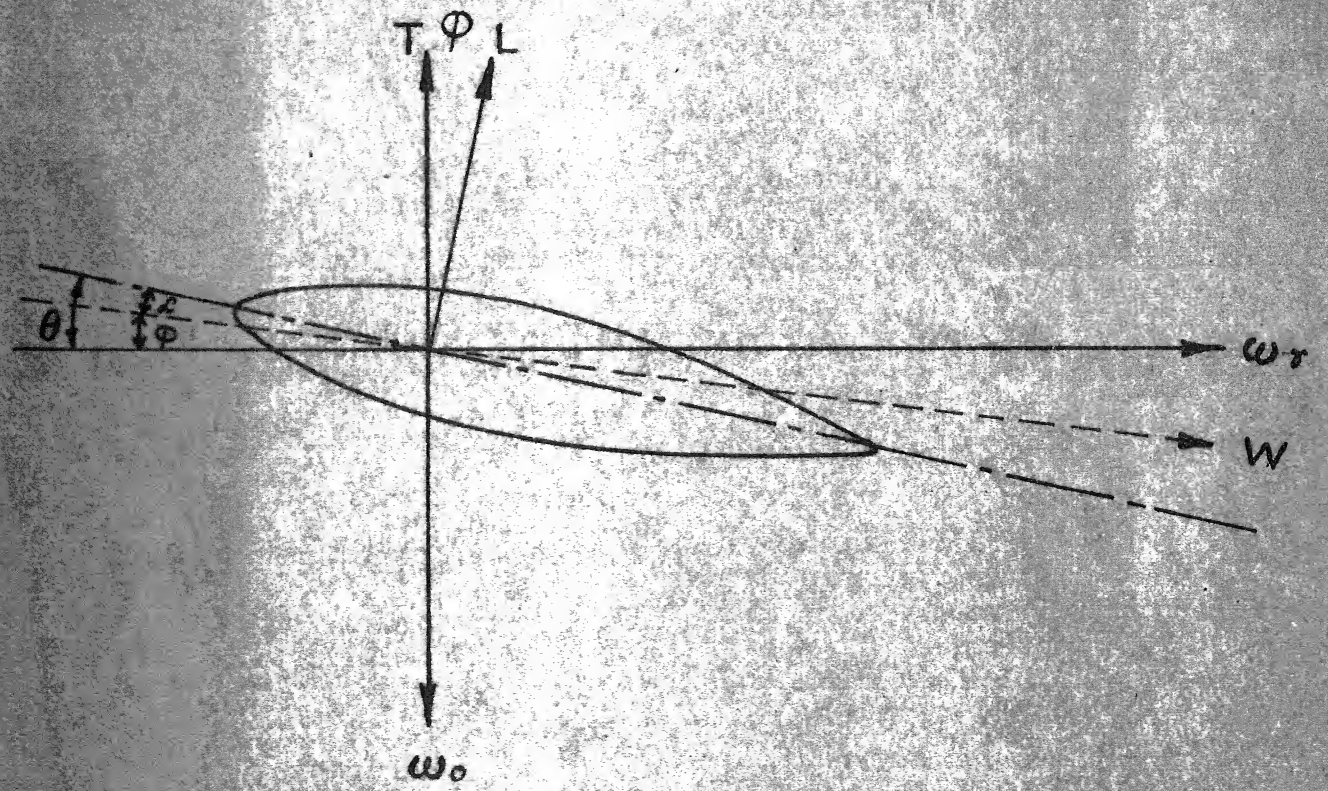

FIG. (3·5·1)

FORCES AND VELOCITIES AT BLADE ELEMENT

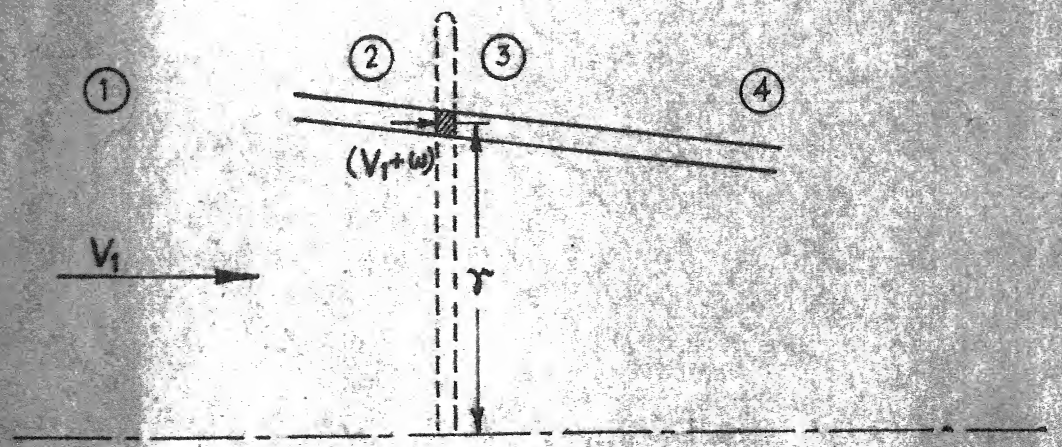

FIG. (4·1·1)

STATION DESIGNATION IN PROPELLER WAKE

FIG. (4·2·1)

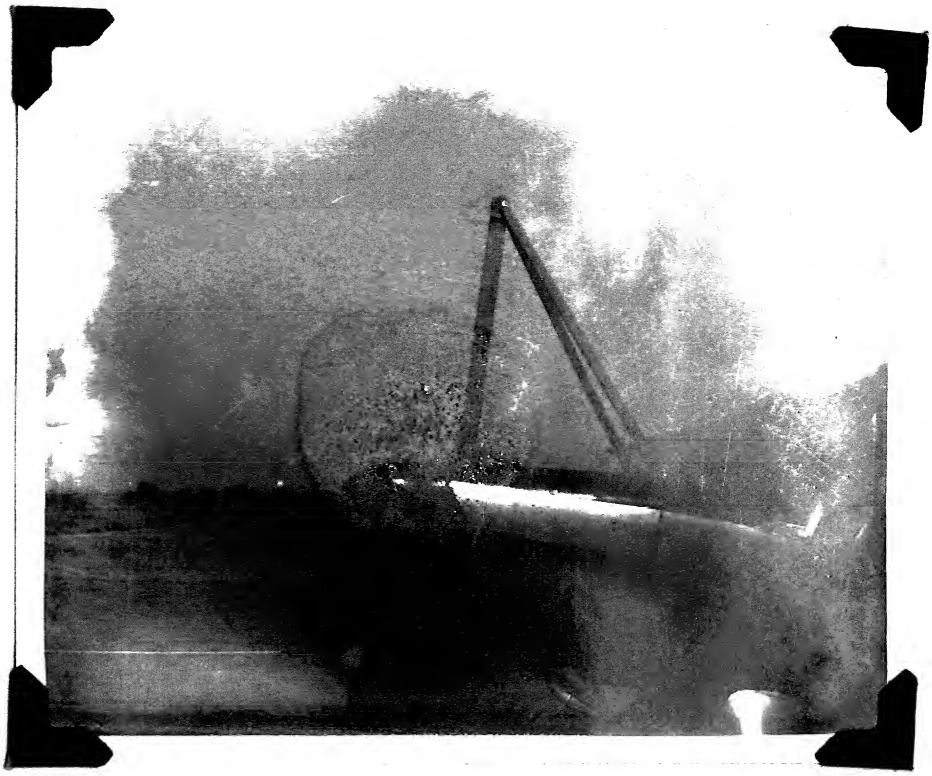

FIG. (4·2·3)

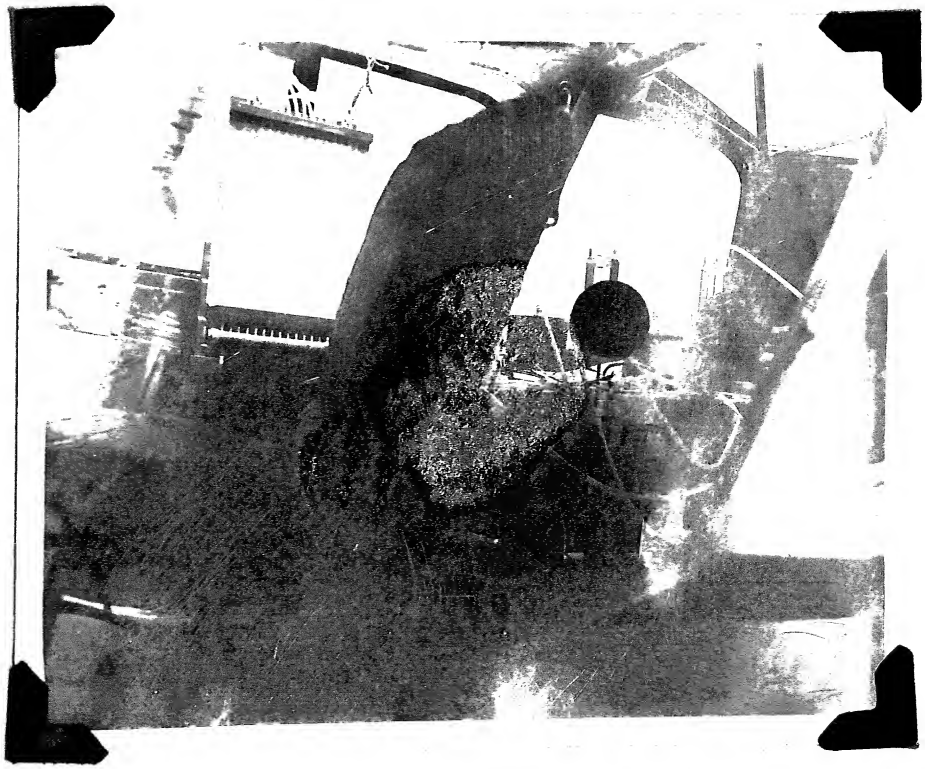

FIG. (4·2·4)

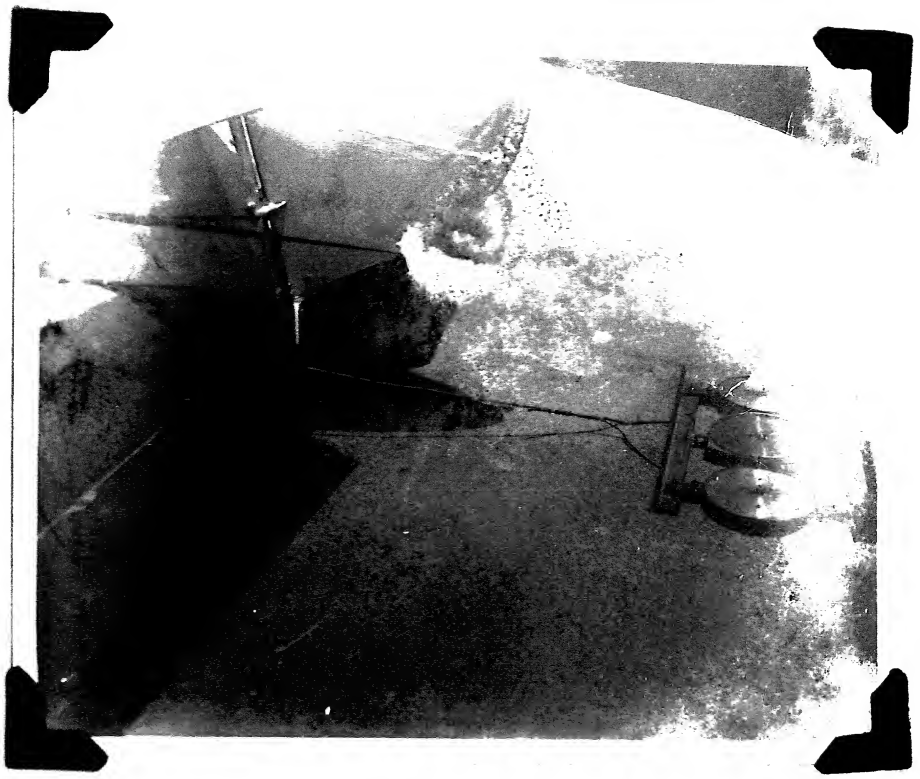

FIG. (4·3·1)

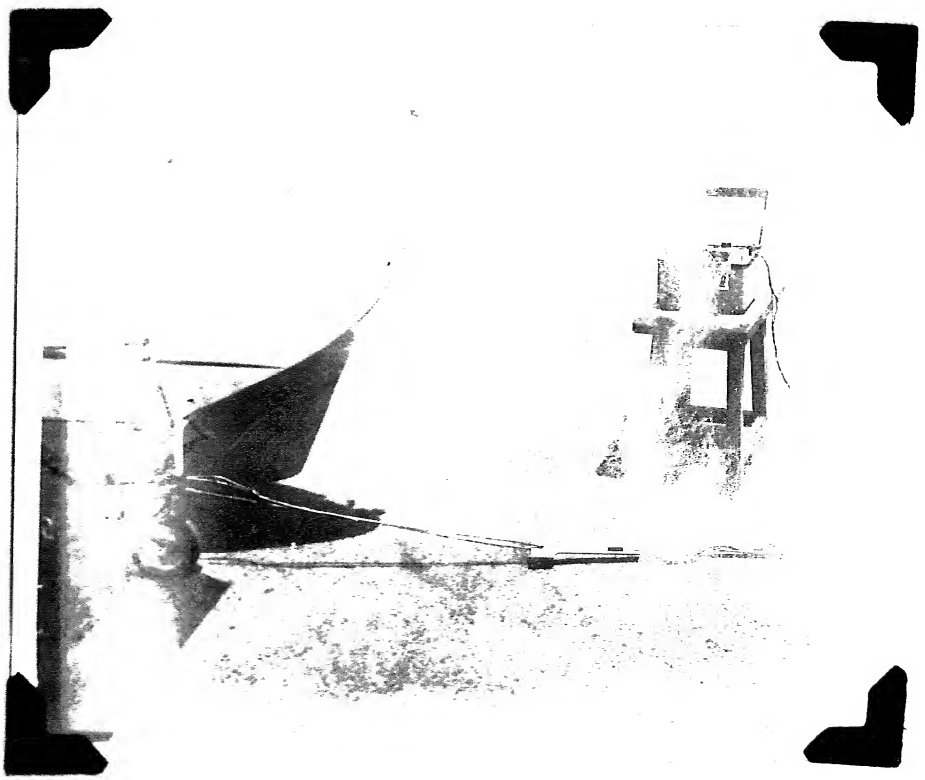

FIG. (4·3·2)

FIG. (433) CALIBRATION OF STRAIN GUAGE

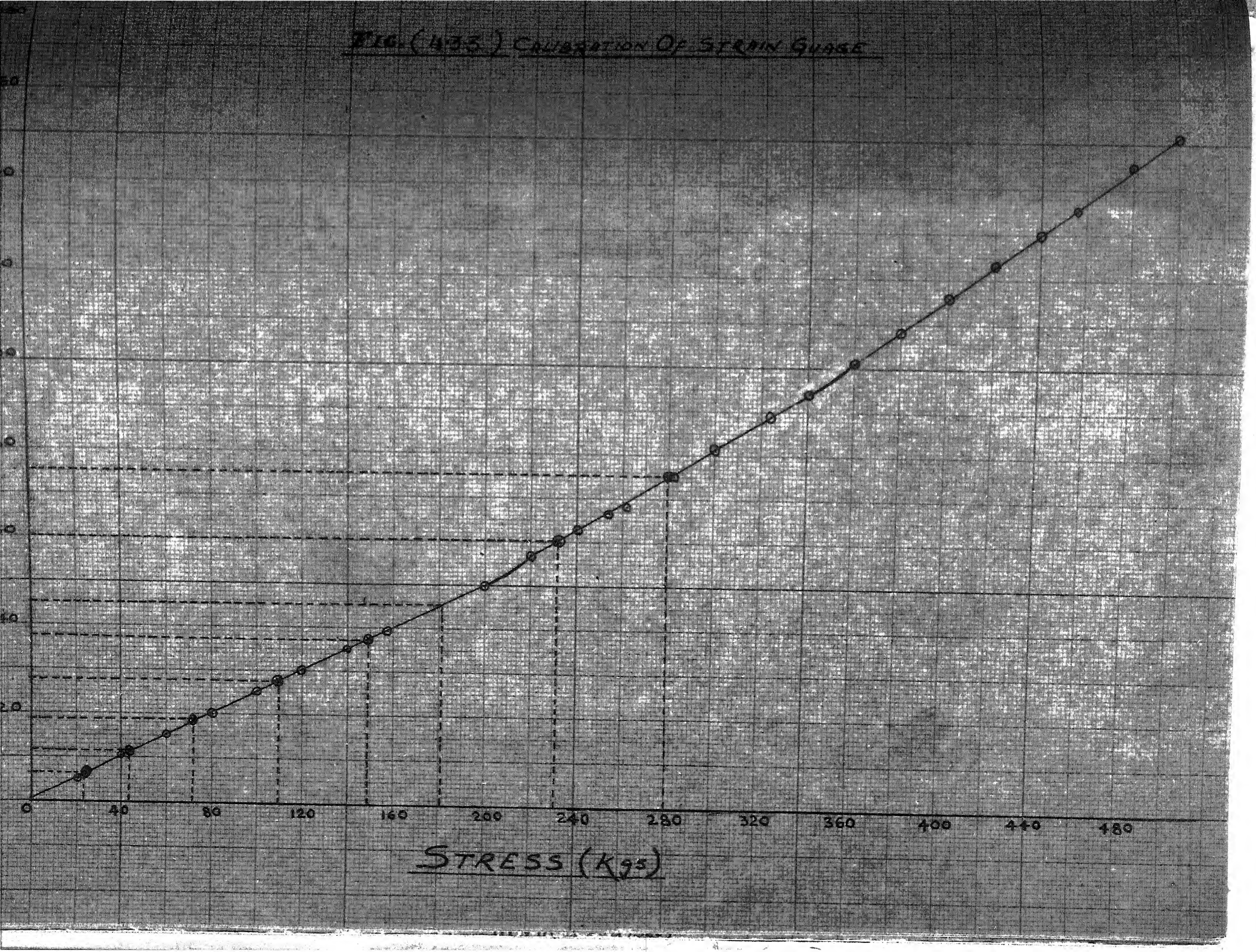

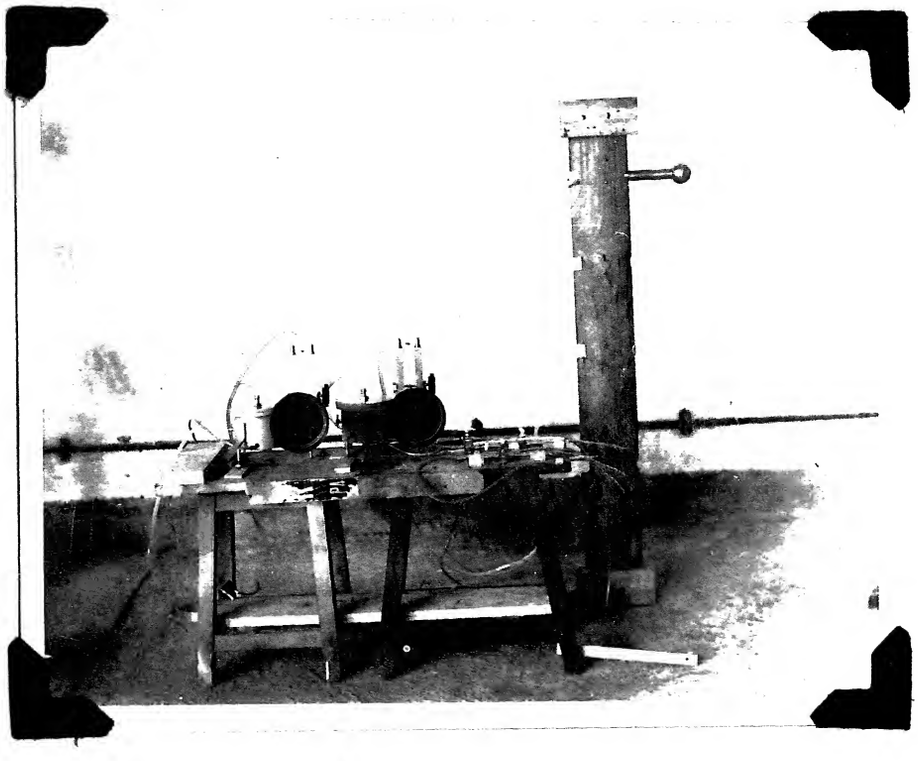

FIG. (4·4·1)

FIG. (4·4·2)

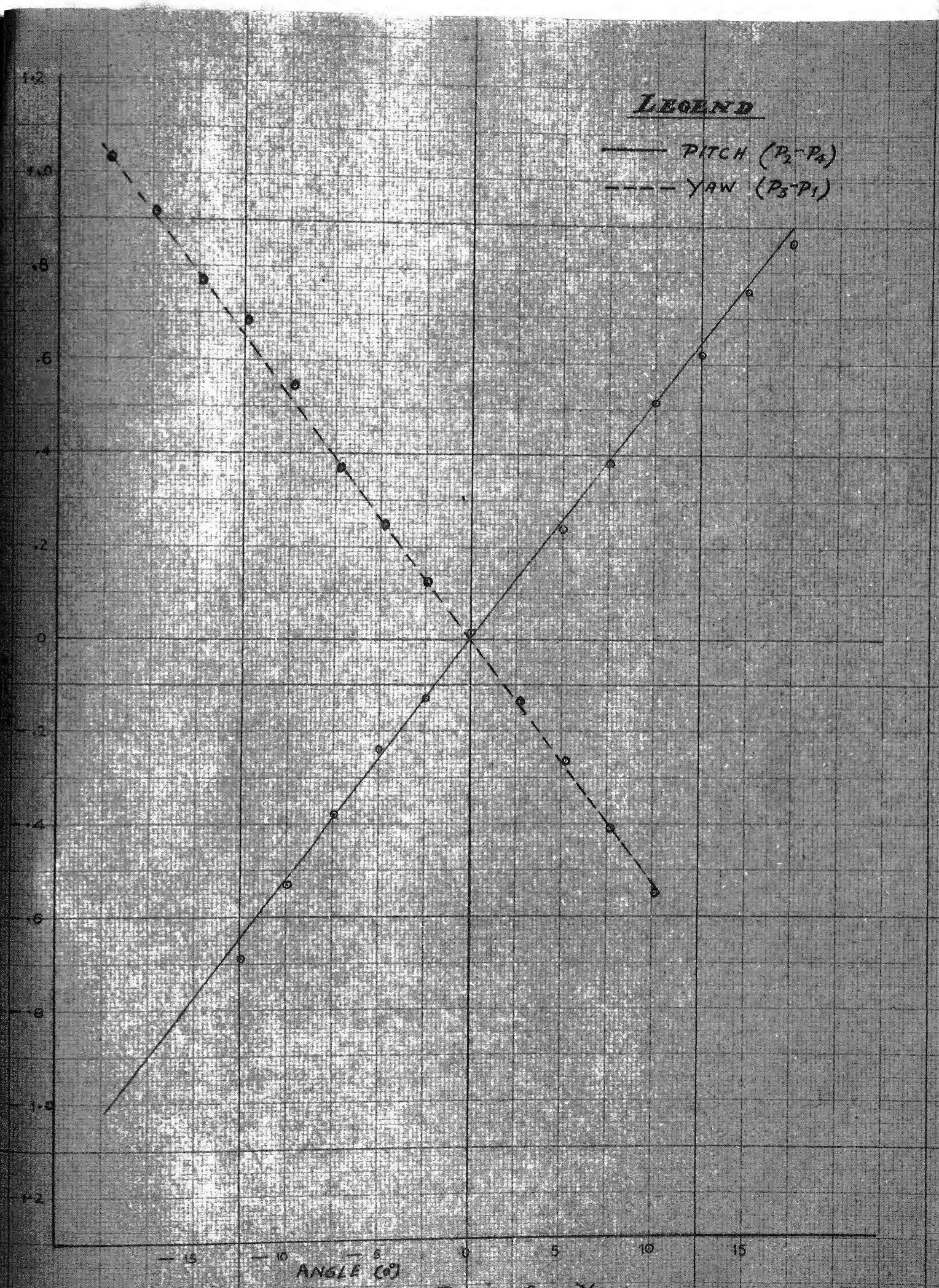

[illegible] PITCH AND YAW

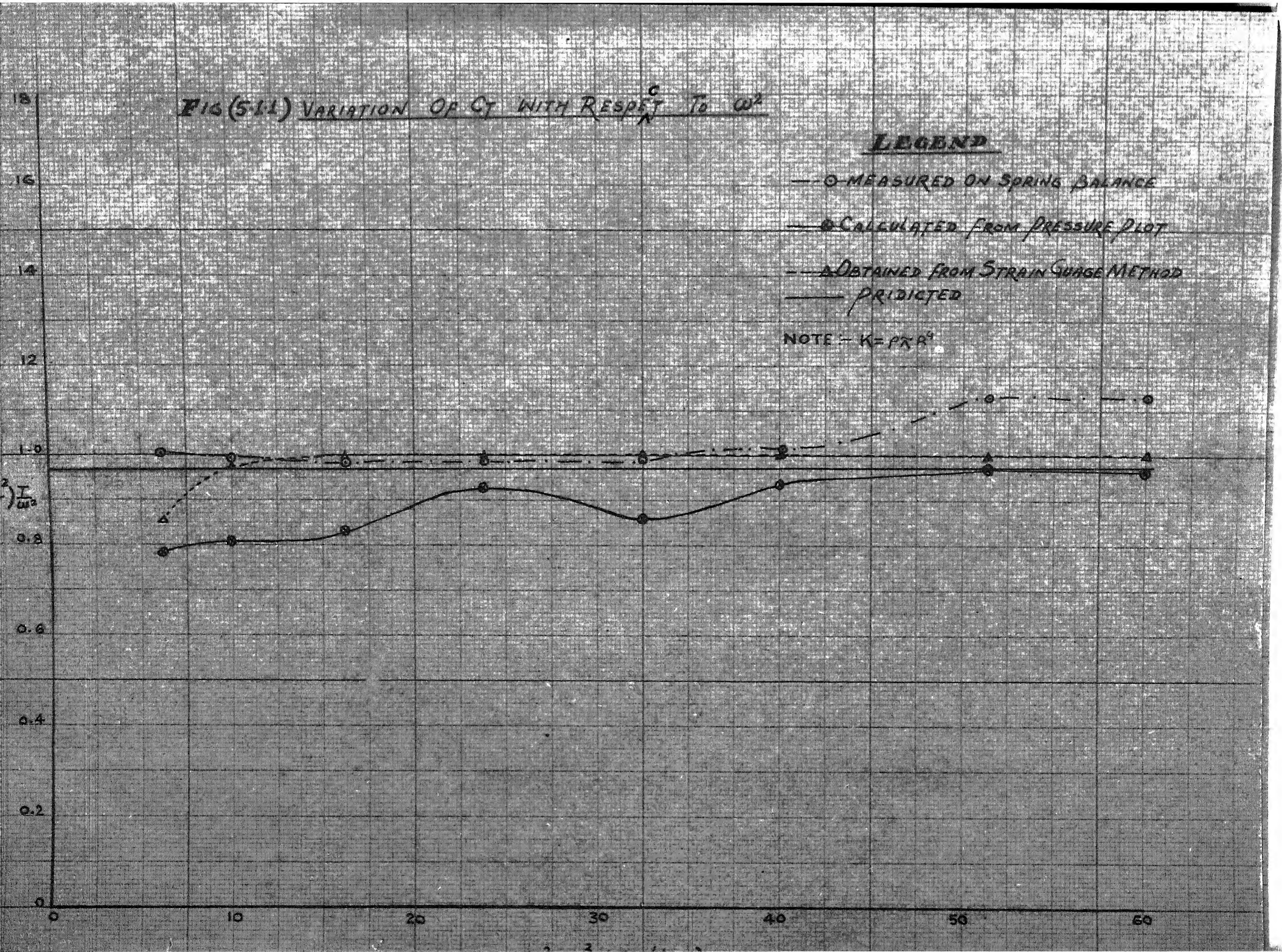
FIG (5.11) VARIATION OF C_T WITH RESPECT TO ω^2
LEGEND
MEASURED ON SPRING BALANCE
CALCULATED FROM PRESSURE PLOT
OBTAINED FROM STRAIN GUAGE METHOD
PRIDICTED
NOTE – $K = \rho \pi R^4$
1.8
1.6
1.4
1.2
1.0
0.8
0.6
0.4
0.2
0
0
10
20
30
40
50
60

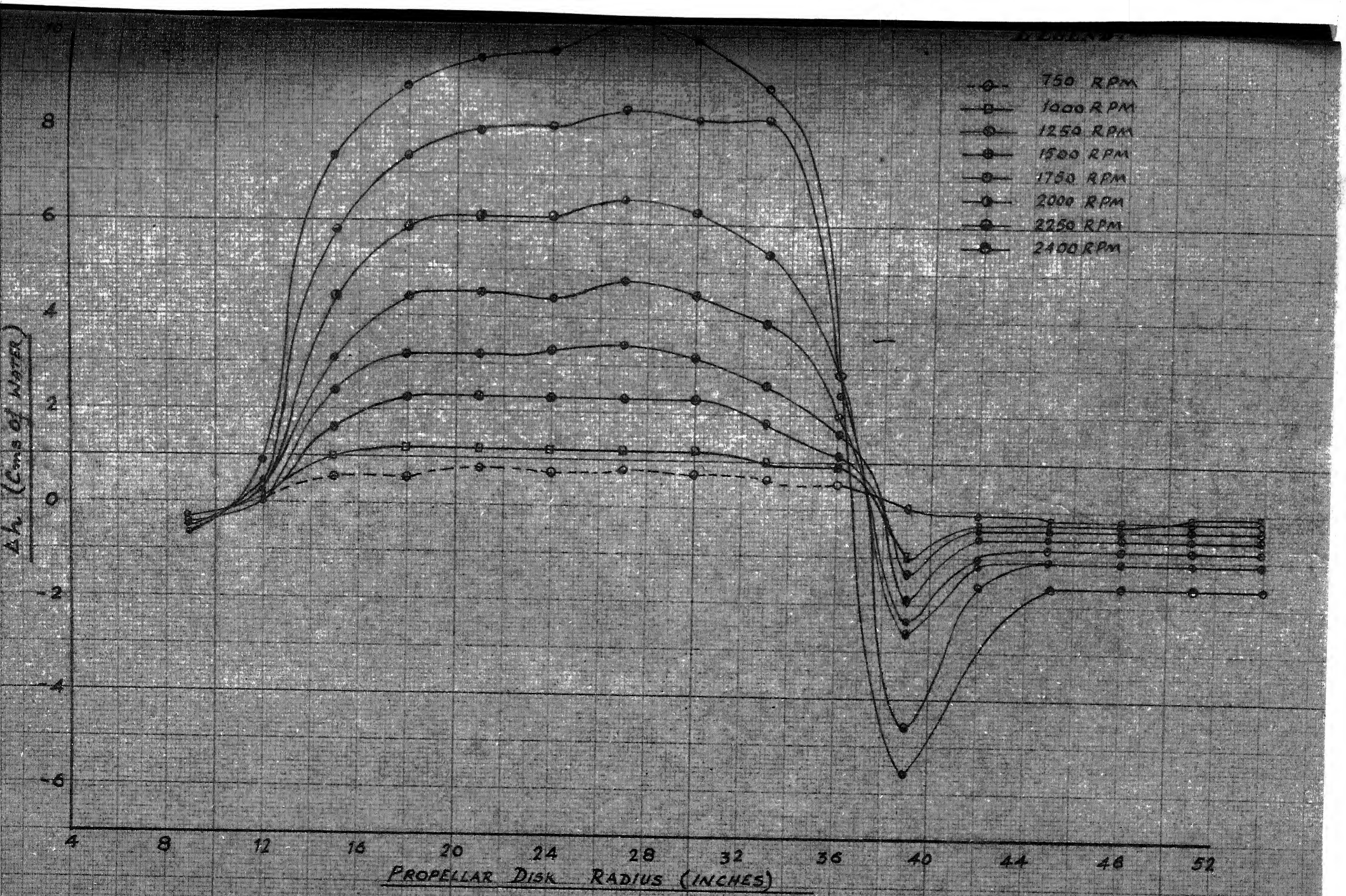

FIG. (5·2·1) PRESSURE RISE ALONG PROPELLAR RADIUS

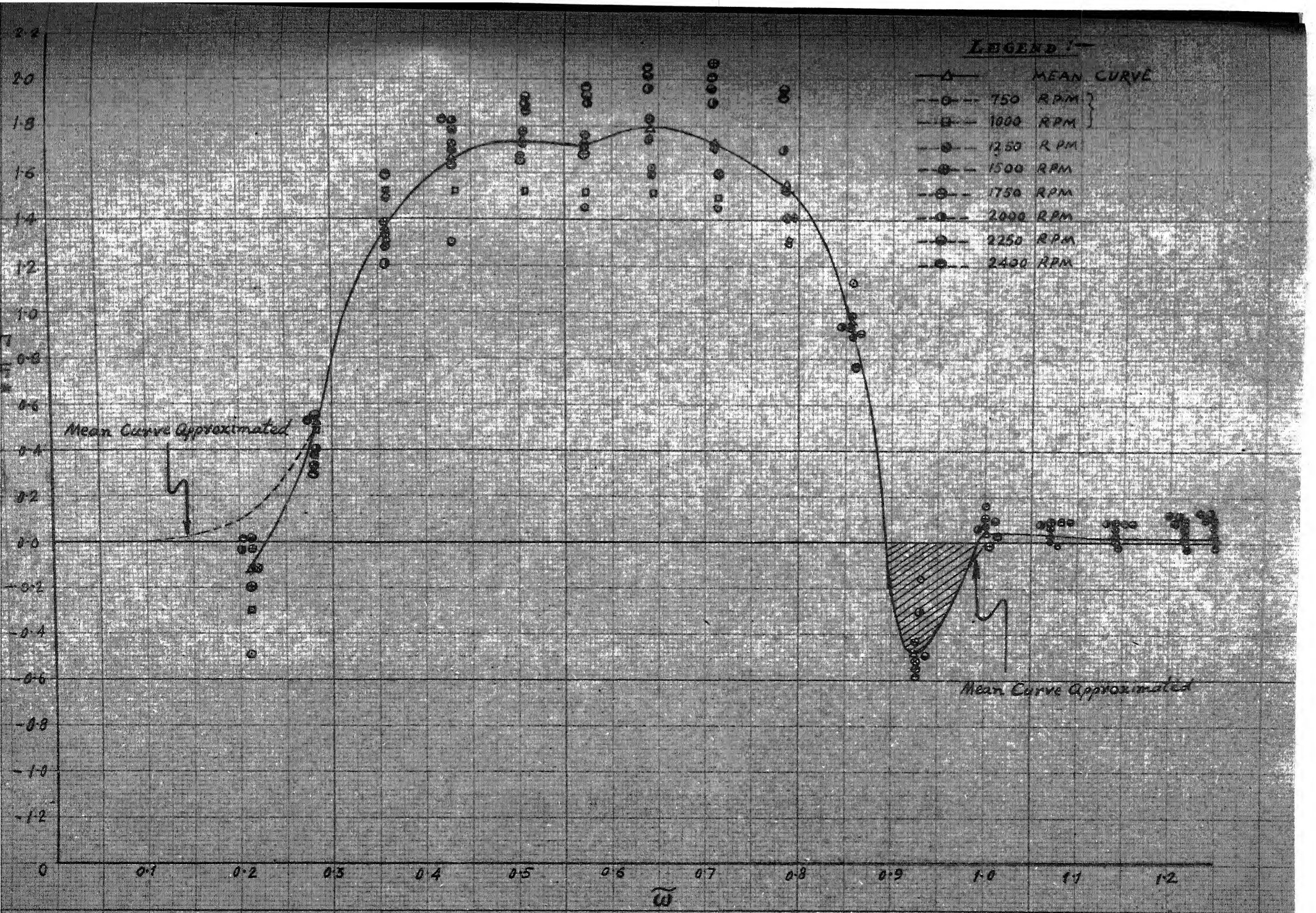

FIG (5·2·2) CIRCULATION VARIATION ALONG RADIUS

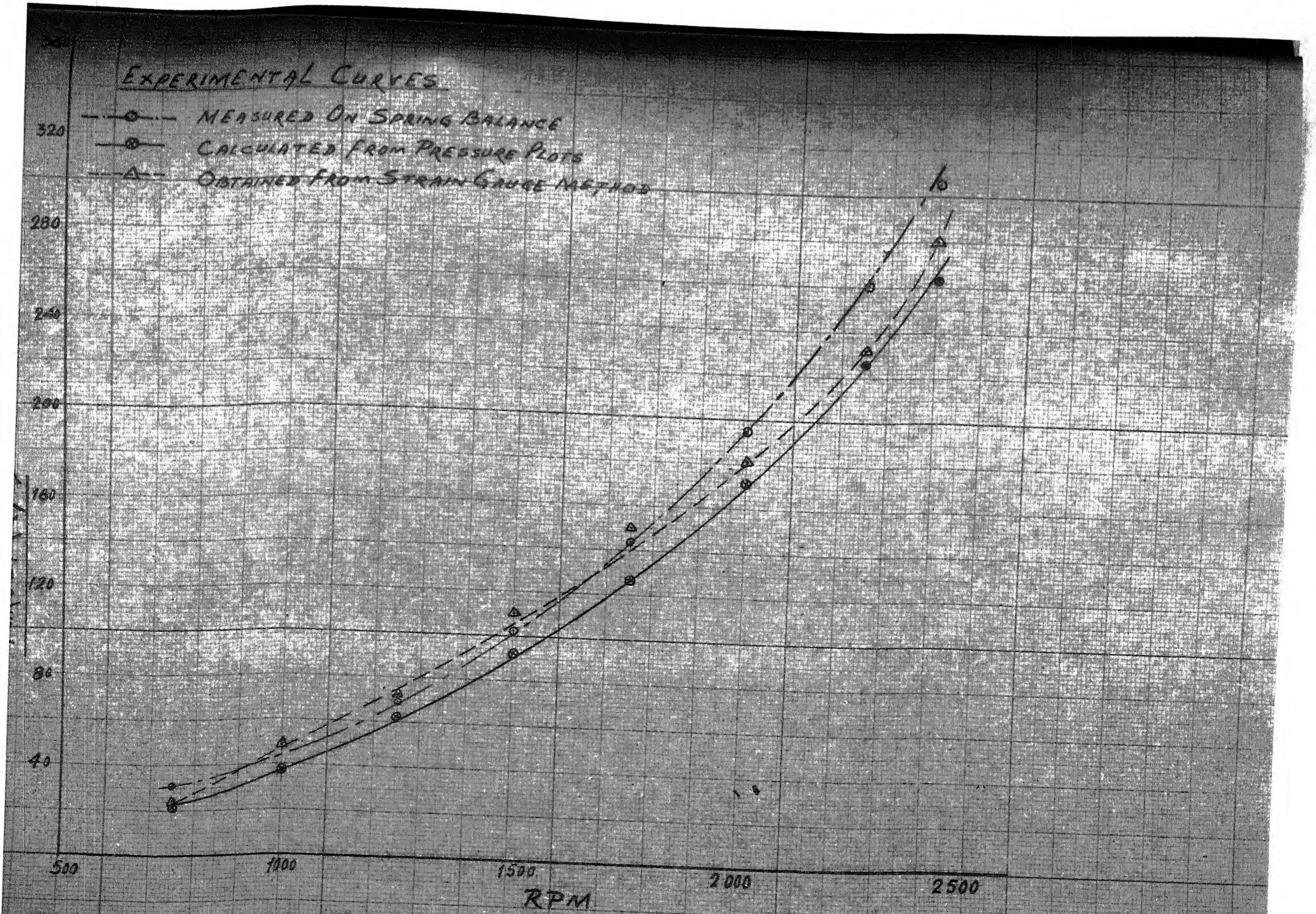

FIG (5.2.3) VARIATION OF THRUST OF PROPELLAR

VARIATION OF THRUST WITH RESPECT TO ω^2 FIG. (5.2.4)

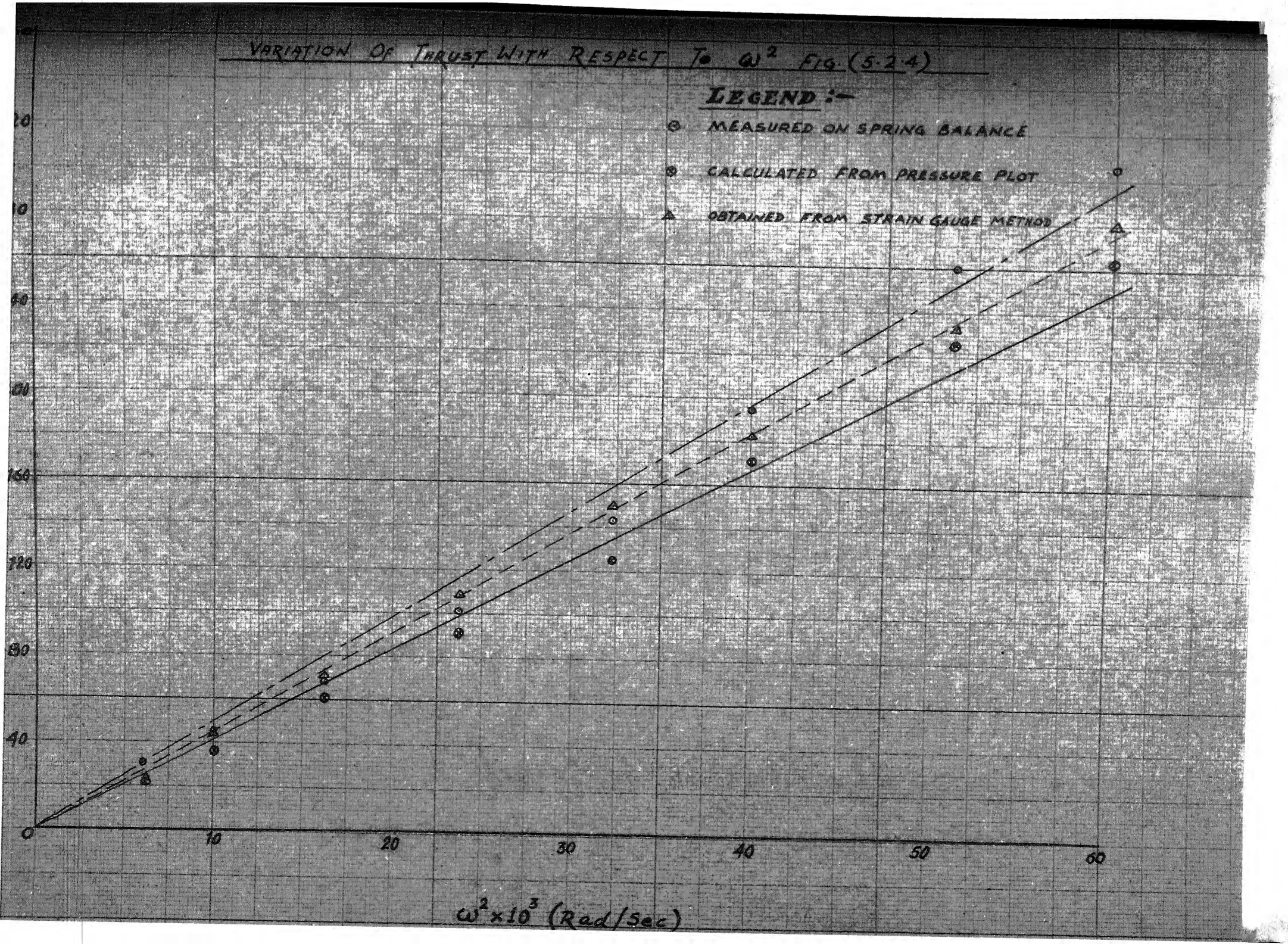

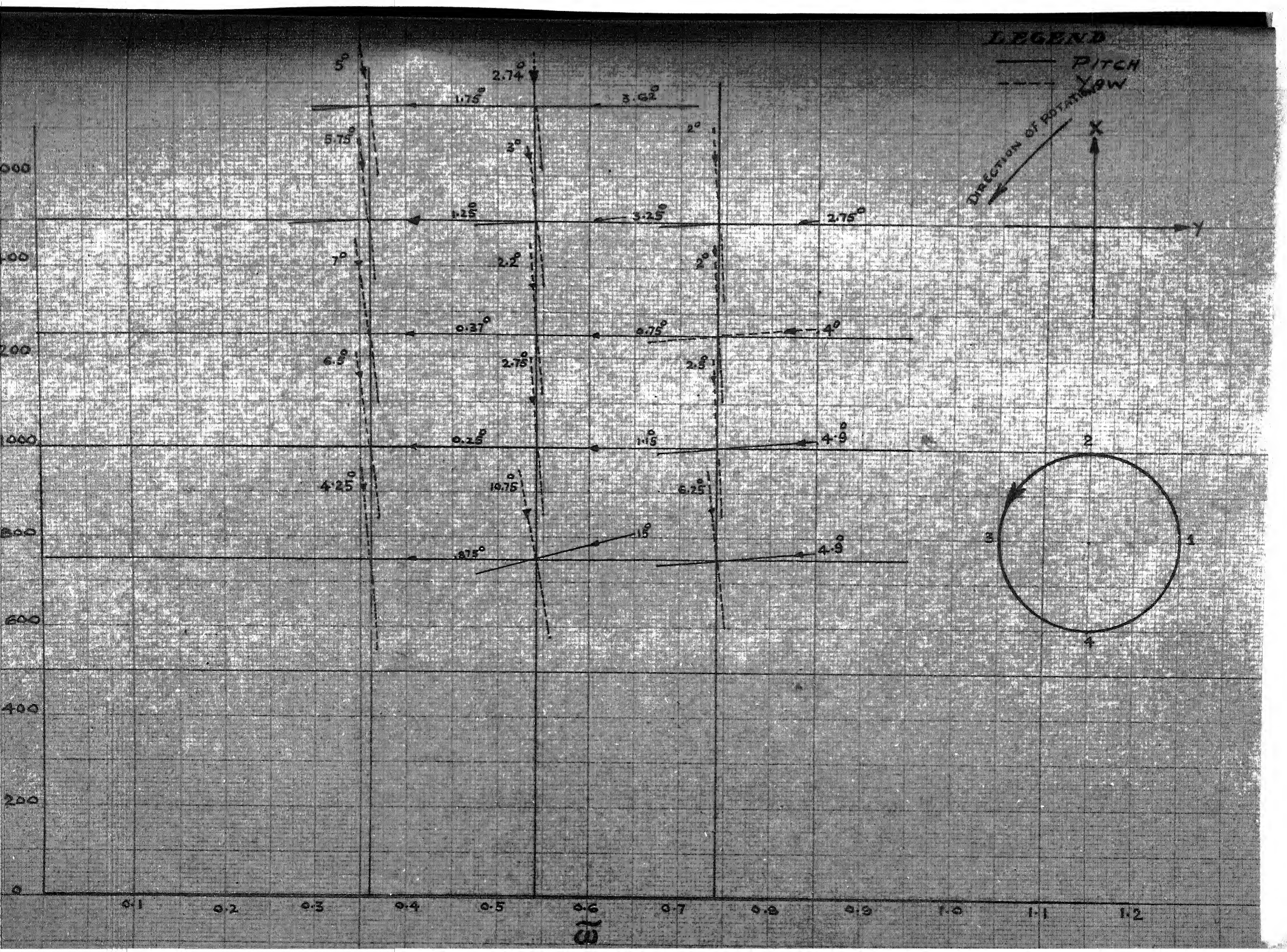
LEGEND
PITCH
YAW
DIRECTION OF ROTATION
X
Y
1
2
3
4
5°
2.74°
1.75°
3.62°
5.75°
3°
2°
1.25°
3.25°
2.75°
7°
2.2°
2°
0.37°
0.75°
4°
6.5°
2.75°
2.5°
0.25°
1.15°
4.9°
4.25°
10.75°
6.25°
1°
.875°
4.9°
0
200
400
600
800
1000
1200
1400
1600
0.1
0.2
0.3
0.4
0.5
0.6
0.7
0.8
0.9
1.0
1.1
1.2
ω̃

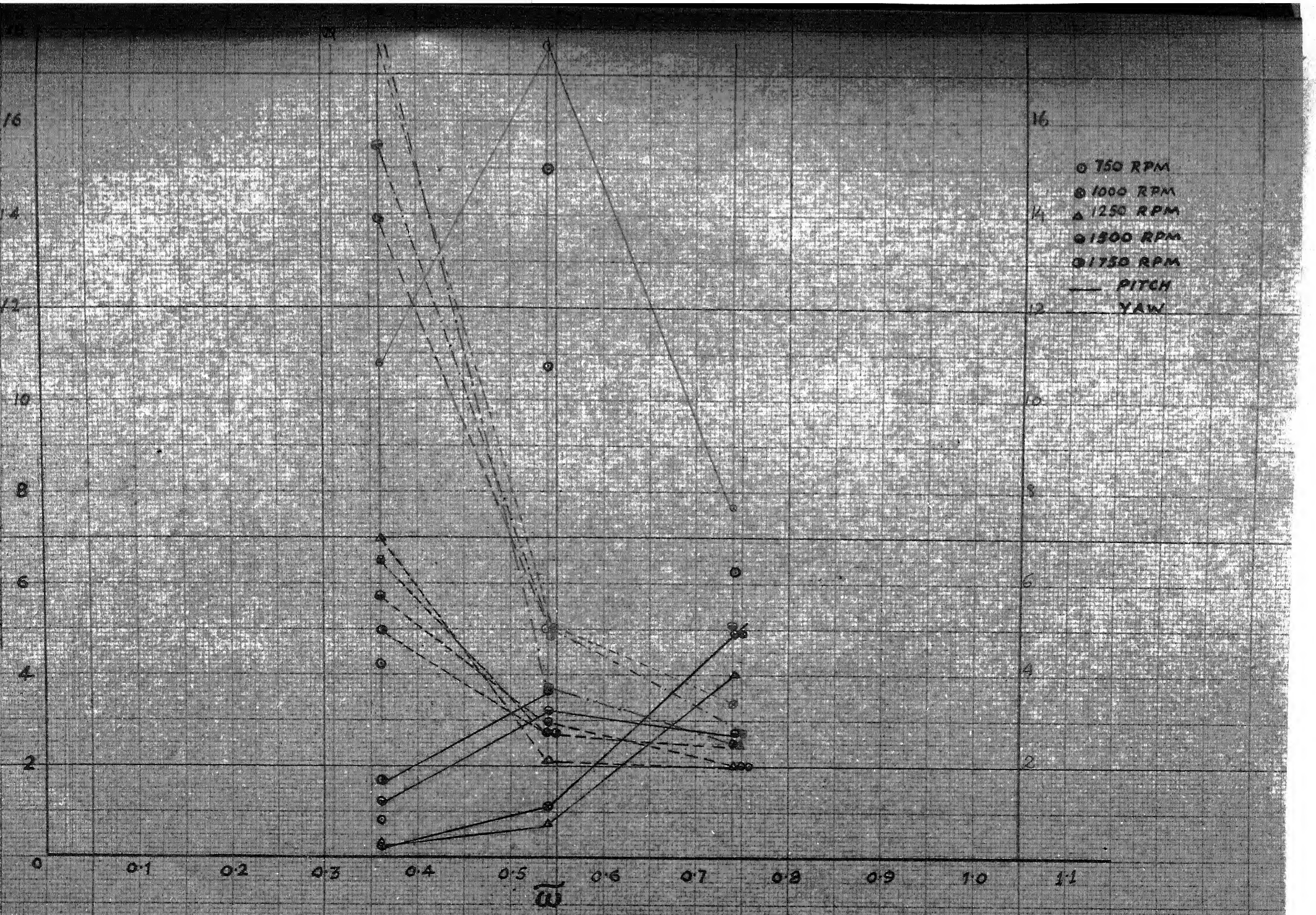

FIG. (5·3·2) SLIPSTREAM INCLINATION